Cyclic ground tilt associated with the 2004–2008 eruption of Mount St. Helens

K. Anderson,[1] M. Lisowski,[2] and P. Segall[1]

Received 4 November 2009; revised 12 April 2010; accepted 25 June 2010; published 6 November 2010.

[1] The long-term behavior of the 2004–2008 effusive eruption of Mount St. Helens was characterized by a gradual decline in the rates of seismicity, dome growth, and broad-scale ground deformation, but shallow near-periodic "drumbeat" earthquakes over timescales of minutes indicated episodic short-term behavior. In part to better characterize this behavior and any associated ground deformation, a network of tiltmeters was installed and recorded thousands of cyclic tilt events within the crater. The duration of these events, from minutes to hours, was too long for them to be directly caused by the drumbeat seismicity. Tilt events were characterized by a recoverable, asymmetric pattern of rapid tilt away from the vent followed by a more gradual reversal, were highly correlated between different tiltmeters in the crater, sometimes occurred in association with volcanic seismicity, and ceased at the end of the eruption. Tilt vectors converged on a point just south of the center of the preexisting 1980s lava dome, and the absence of detectable tilt outside the crater suggests a shallow source (<1 km). We examine several models, including cycles of conduit pressurization and plug slip or gas loss and stick-slip behavior on the interface between the ascending plug and the 1980s lava dome. The small number of stations within the crater prevents a unique determination of source type or geometry, but results are consistent with a mechanism involving extrusion of the semisolid dacite plug and/or cycles of conduit pressurization.

Citation: Anderson, K., M. Lisowski, and P. Segall (2010), Cyclic ground tilt associated with the 2004–2008 eruption of Mount St. Helens, *J. Geophys. Res.*, *115*, B11201, doi:10.1029/2009JB007102.

1. Introduction

[2] At silicic volcanoes, magmatic processes in the upper conduit play an important role in governing eruptive behavior. At shallow depths, magma degassing and crystallization may dramatically increase the viscosity of the melt, creating a plug of solid or semisolid rock which acts to resist flow and thereby exerts a critical control on eruption evolution. While seismicity may be used to study shallow conduit processes, ground deformations are often too difficult to measure near the vent because of their small size and because of the danger in placing instruments in this area. Instead, broad-scale ground deformation data are typically used to infer properties of the magma chamber feeding the eruption, not extrusion processes near the top of the conduit.

[3] Tiltmeters are well suited for measuring the often weak ground deformations associated with transient upper conduit processes, but although these instruments have been successfully deployed at many volcanoes around the world, few well-documented cases exist of tiltmeters installed close to the vents of erupting silicic volcanoes. Examples include Mount St. Helens in the 1980s, where tiltmeters were used to predict effusive eruptions [*Dzurisin et al.*, 1983], and Soufriere Hills Volcano (Montserrat), where tiltmeters revealed remarkable cyclic eruptive activity correlated with seismicity, gas emissions, explosions, and pyroclastic flows [*Voight et al.*, 1998; *Watson et al.*, 2000] and helped place constraints on source processes and boundary conditions on the conduit walls [*Green et al.*, 2006; *Widiwijayanti et al.*, 2005; *Voight et al.*, 1999; *Lensky et al.*, 2008]. Cyclic or repeating behavior on a variety of timescales has also been observed with different types of instruments during other silicic eruptions including Mount St. Helens during the 2004–2008 eruption [*Iverson et al.*, 2006], Pinatubo [*Mori et al.*, 1996], Santiaguito [*Bluth and Rose*, 2004], and Unzen [*Nakada et al.*, 1999].

[4] Because the eruption of Soufriere Hills Volcano has been so well documented and because of the remarkable nature of the cyclic behavior observed, the eruption has been the focus of much modeling. Most models have ascribed cyclic behavior to periods of degassing-induced rheological changes in a relatively stiff magma plug underlain by a compressible, pressurized melt. *Wylie et al.* [1999] model viscosity changes due to degassing as melt nears the surface; for steady influx, this can produce pressure and slip cycles. *Lensky et al.* [2008] include the effects of gas loss as well as nonlinear friction on the margins of the plug, and ascribe tilt cycles to influx of new material and short-timescale pressurization

[1]Department of Geophysics, Stanford University, Stanford, California, USA.
[2]USGS Cascades Volcano Observatory, Vancouver, Washington, USA.

0148-0227/10/2009JB007102

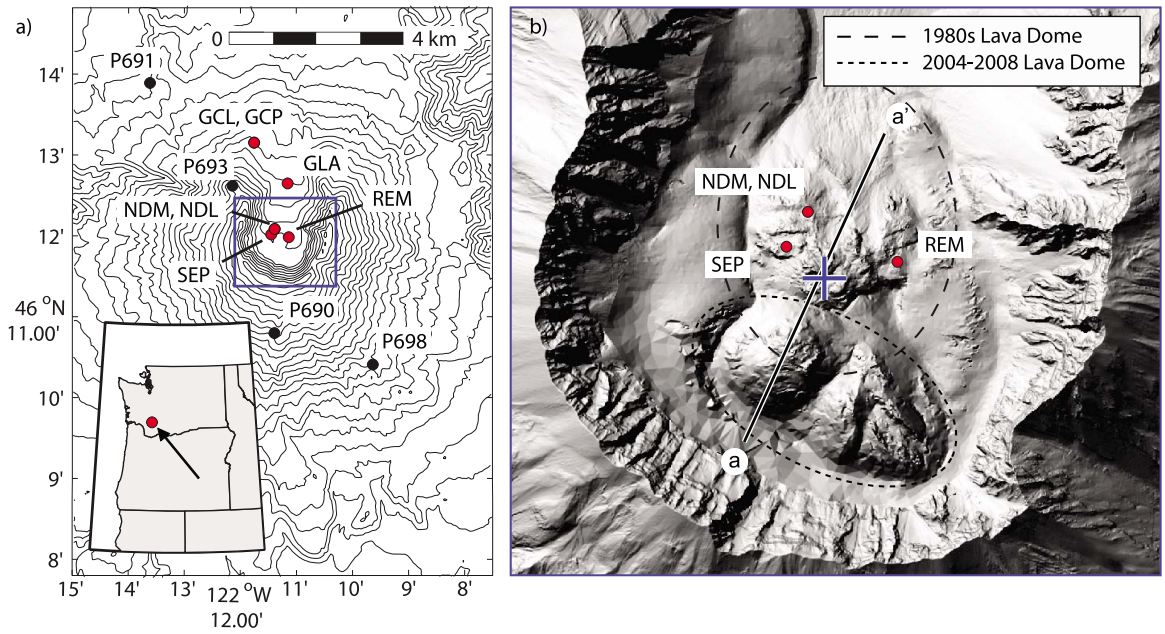

Figure 1. Tilt network at Mount St. Helens, 2005 to 2008. Not all stations were concurrently operational. (a) Contour map of Mount St. Helens showing PBO stations (with "P" prefix) and U.S. Geological Survey stations. Box shows approximate location of enlargement in Figure 1b, and inset shows location of Mount St. Helens in Washington State. (b) Enlarged shaded relief map of the crater showing 1980s and recent lava domes as they appeared in February 2006. Outline of old dome is based on its dimensions before the formation of the glacier in the crater and is approximated from *Vallance et al.* [2008]. Line from points a to a′ shows approximate location of the cross section in Figure 2. Cross shows approximate center of radial coordinate system used throughout this paper.

due to gas exsolution beneath a solid plug. At Mount St. Helens, *Iverson et al.* [2006] model periodic seismicity as due to slip on a solid magma plug underlain by compressible magma.

[5] Further examples of cyclic behavior are needed to better constrain these models and clarify processes of magma ascent and extrusion, and the way these processes give rise to surface deformation. The relatively extensive network of tiltmeters in operation during the 2004–2008 eruption of Mount St. Helens, and the thousands of transient, cyclic, near-vent ground tilt events which they captured in remarkable detail, provide a unique opportunity to examine and model shallow eruptive processes during the long-term, stable eruption of a silicic volcano, and provide a useful case study for comparison with Soufriere Hills Volcano.

2. The 2004–2008 Eruption of Mount St. Helens

[6] Mount St. Helens (MSH), located in southwestern Washington State (Figure 1a), has been the most frequently active volcano in the Cascades for the past several thousand years [e.g., *Scott et al.*, 2008]. The volcano erupted with a catastrophic landslide and lateral blast in 1980. This event excavated a large horseshoe-shaped crater in which dome-forming eruptions continued until 1986. After nearly 20 years of quiescence, and following only a few days of increased seismic activity [*Moran et al.*, 2008a], Mount St. Helens began to erupt again in October 2004. The eruption continued until early 2008 and was characterized by the effusive growth of a large dacitic lava dome in the crater between the most recent (1980s) dome and the south crater wall (Figure 1b) [*Vallance et al.*, 2008]. The growth rate of the dome declined quasi-exponentially from ~8 m^3/s [*Schilling et al.*, 2008; S. Schilling, personal communication, 2010] until the cessation of the eruption. GPS data collected around the volcano suggest that the eruption was fed by a deflating ellipsoidal magma reservoir centered at 7–8 km depth [*Lisowski et al.*, 2008; *Mastin et al.*, 2008].

[7] The site of initial phreatic explosions and the earliest extrusion appears to have been on the south facing slope of the 1980s lava dome, buried beneath the crater glacier [*Vallance et al.*, 2008]. The first spine protruded through the glacier on 11 October 2004 [*Vallance et al.*, 2008]. Rock extruded throughout the eruption consisted of ~65% SiO_2 dacite with 40–50% phenocrysts. Petrologic evidence, including the low volatile content of matrix glasses, suggests that crystallization of the matrix occurred at shallow depths (<~1 km) [*Pallister et al.*, 2008]. The resulting plug of near-solid rock was then forced upward through the vent and extruded onto the surface as a series of recumbent spines. These spines typically broke up during emplacement and were overridden by new spines. Spine 3 (the third major spine extruded during the eruption) showed a smooth rounded exterior and was termed a "whaleback," the rounded surface of which provided an estimated vent diameter of ~100–200 m [*Pallister et al.*, 2008]. Spines often displayed a ~1–3 m thick veneer of fault gouge with slickenside striations [*Cashman et al.*, 2008], suggesting that shear of the ascending plug was localized to a thin annular shell. Figure 2 shows a simple

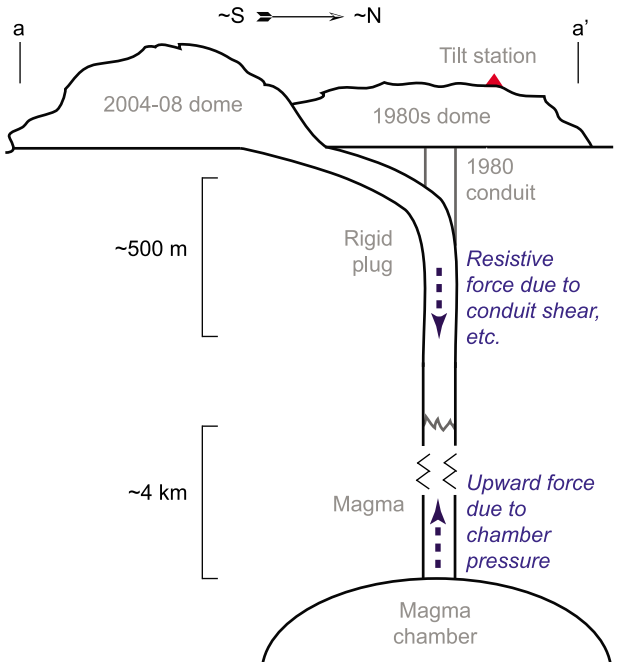

Figure 2. Schematic cross section showing geometry of 1980s and 2004–2008 lava domes, diversion of plug to the south beneath the 1980s dome, and simple force balance between magma chamber overpressure and near-surface conduit resistance. Not drawn accurately to scale. Approximate location of cross section is shown in Figure 1b.

schematic cross section of magma ascent and plug extrusion beneath MSH.

[8] GPS instruments recorded Spine 3 moving southward during November 2004 at up to 10 m/d [*LaHusen et al.*, 2008]. The 1980s lava dome (the "old dome") also moved, although at a much lower rate; through the early part of 2005, it moved northward away from the site of new extrusion as a semicoherent block at up to 2 cm/d. This velocity appeared to correlate with extrusion rate of the new lava dome, and the velocity of the 1980s dome sometimes appeared to increase along with real-time seismic amplitude measurements (RSAM) [*LaHusen et al.*, 2008].

[9] More than one million shallow earthquakes were recorded at MSH between the onset of the eruption and the end of 2005 [*Moran et al.*, 2008a; *Thelen et al.*, 2008]. Initial seismicity consisted largely of volcano-tectonic (VT) earthquakes but soon transitioned to low-frequency (LF) and hybrid events (those with a high-frequency onset but transitioning to lower frequencies), following a pattern observed at many dome-building eruptions [*Moran et al.*, 2008a] including at MSH in the 1980s. Earthquakes were mostly located <1 km below the crater floor, and very early in the eruption exhibited temporal shallowing on a north dipping structure likely coincident with the shallow conduit [*Thelen et al.*, 2008]. Remarkable features of seismicity at MSH included the prevalence of multiplets as well as remarkably periodic hybrid events termed "drumbeats." Hybrid earthquakes were interpreted by *Harrington and Brodsky* [2007] as brittle failure events involving low rupture velocities and strong path effects. *Iverson et al.* [2006] modeled the drumbeat events as caused by repeating slip on the margin of the ascending magma plug. *Waite et al.* [2008] however, analyzed long-period seismic events recorded during the summer of 2005, and concluded that these events were inconsistent with a shear-faulting source and suggested instead the repetitive opening and closing of a steam- or fluid-filled crack or cracks located beneath the growing lava dome. *Waite et al.* [2008] also analyzed very long period (VLP) events (periods of 15–25 s) during the same time and suggested that the source mechanism for these events involved the contraction and expansion of a sill and dike system located beneath the SW edge of the 1980s lava dome.

[10] Seismicity, dome growth, and broad-scale ground deformation rates all declined throughout the eruption. By the time of the first tiltmeter installation in fall of 2005, extrusion rates had declined to roughly 1 m^3/s [*Schilling et al.*, 2008], and roughly two thirds of the broad-scale ground deformation recorded during the eruption had already occurred (Figure 8a). By January 2008 cameras monitoring the dome detected no further growth, gas emission and earthquake rates dropped to nearly zero, and the episodic ground tilts which are the focus of this work ceased, marking the end of the 2004–2008 eruption [*Cascades Volcano Observatory*, 2008].

3. Data and Processing

3.1. Tilt Network

[11] The U.S. Geological Survey Cascades Volcano Observatory (CVO) operated seven tiltmeters at five locations at Mount St. Helens during the 2004–2008 eruption, with most data recorded at 1 Hz and telemetered out of the crater (Figures 1 and 3 and Table 1). Over the course of the eruption, between two and four tiltmeters were typically operational simultaneously. Three tiltmeter sites (REM, SEP, and NDM/NDL) were located on the old 1980s lava dome, while two more sites were located farther from the vent (GLA and GCL/GCP). Tiltmeters were electronic self-leveling instruments installed in shallow (~1 to 6 m) boreholes. Most CVO tiltmeters were Pinnacle Technologies Series 5000 instruments, but two Applied Geomechanics LILY tiltmeters were installed as a check of instrument response and data validity: one (NDL) sharing a borehole with a Pinnacle instrument (NDM) on the 1980s lava dome at North Dome, and another (GCL) installed close to a Pinnacle instrument (GCP) several kilometers north of the crater at Guacamole. Each station recorded ground tilt in

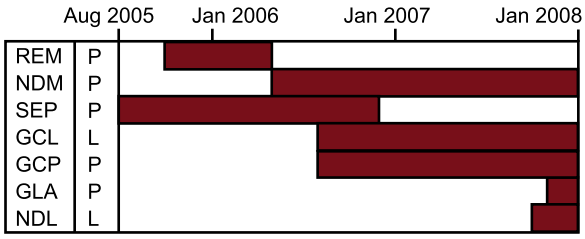

Figure 3. Operational periods of CVO tiltmeters installed at Mount St. Helens through January 2008. Tiltmeter types P, Pinnacle; and L, LILY are shown.

Table 1. Locations and Installation Depths of CVO Tiltmeters[a]

Station	East (m)	North (m)	Elevation (m)	Depth (m)
NDM	-	-	2070	2.5
NDL	-	-	2070	~1
REM	+327	−183	2109	1.8
SEP	−78	−125	2130	2.3
GCL	−490	+1970	1630	6
GCP	−490	+1970	1630	6
GLA	+286	+1050	1712	2.0

[a]Distances east and north are measured relative to the position of NDM/NDL. Elevations are approximate orthometric height. Depth is installation depth at the base of the tiltmeter.

two orthogonal directions, and most stations were installed such that the y axis pointed generally away from the growing lava dome; in this orientation, a positive y tilt indicates tilt away from the new dome. Additionally, the Plate Boundary Observatory (PBO) operated several tiltmeters on the flanks of the volcano during the eruption, although these stations experienced technical problems for much of the eruption.

[12] The different tiltmeters installed at MSH applied different internal smoothing filters to the data before transmission, which can substantially alter the response of the instruments to short-period signals such as teleseismic waves. Three of the Pinnacle instruments (NDM, GLA, and GCP) applied ~30 s internal analog smoothing filters, while the Pinnacle instruments at SEP and REM were modified to apply a shorter-period smoothing filter. The LILY instruments averaged over 1 s.

3.2. Data Processing and Verification

[13] Tiltmeter data must be interpreted with significant caution. In addition to the tilt signal of interest, tiltmeters may record real and/or apparent ground tilt due to temperature changes (from temperature sensitivity of the sensor as well as thermoelastic strain in the near surface [*Bonaccorso et al.*, 1999]), barometric pressure changes, rainfall, instrument settling, and local topography causing strain-tilt coupling [*Meertens and Wahr*, 1986]. Additionally, recorded tilts may differ from theoretical predictions due to material heterogeneity, topography, cavity effects (in which the borehole itself alters the strain field), and poor coupling and/or differential motion between the instrument and the borehole [*Kohl and Levine*, 1993]. Additional uncertainty lies with the orientation of the tiltmeter in the ground (orientations at MSH were estimated in the field during installation, and also using the tiltmeters' internal magnetic compasses), the possibly nonlinear response of the tiltmeter to shaking caused by local earthquakes, and any potential defects with the tiltmeter itself.

[14] Because of these uncertainties it is critical to verify tiltmeter data by comparing different instruments to one another and by comparing instrument response to known signals. The presence of a 1 Hz tiltmeter network at MSH including colocated instruments as well as instruments of different manufacture has allowed us to check the recorded tilt signals in ways that are impossible with a smaller, less diverse network. We examined the response of the tiltmeters to teleseismic and microseismic waves, diurnal and semidiurnal ground tilt, temperature changes, the episodic ground tilt that is the focus of this work, and other signals. We also manually rotated two of the instruments in their borehole in order to validate the instrument response.

[15] We find that most stations appeared to operate correctly (installation orientations were largely correct, electronics gain settings were consistent between instruments across the network, and colocated stations recorded similar signals at periods of seconds and hours in the absence of significant ground shaking) but that colocated tiltmeters installed at North Dome (NDM and NDL) differed substantially in their response to a variety of ground tilts. Episodic tilt events (which occurred at periods between those of teleseismic waves and diurnal signals, which we used to verify the instruments) were recorded at NDM with an amplitude and azimuth consistent with other instruments installed on the 1980s lava dome, but at the shallower station installed at North Dome (NDL) these tilts were detected weakly, if at all. We believe that due to its very shallow depth NDL was strongly influenced by surface effects such as local cracks, and may also have been influenced by its proximity in the borehole to the cable connecting NDM (below it in the borehole) to the surface. Based on our analysis we largely disregard tilt data from this station; details of instrument and data verification are given in Appendix A.

[16] Routine data processing included spike and offset removal, filtering to remove long-period signals (usually with a cutoff of ~8 h) and, for directly comparing data between stations with different smoothing filters, application of a simple smoothing filter (approximately equivalent to a 30-s low-pass filter) to the data from "unfiltered" stations. To assist in this work, we developed the software package MATILDA (from "MATLAB Tilt Data Analysis") for the processing, display, and analysis of tiltmeter data, and this code is freely available.

4. Ground Tilt at Mount St. Helens

[17] With eleven tiltmeters (including the PBO stations) operating variously at nine different locations over the course of 3 years, a complex picture of ground tilt at Mount St. Helens has emerged. In this work we focus on thousands of remarkable correlated episodic ground tilts which were clearly detected on tiltmeters located on the 1980s lava dome over the course of the eruption.

[18] The first CVO tiltmeter (SEP) was installed at Mount St. Helens just under 1 year after the start of the eruption, in August 2005. Large tilt spikes associated with drumbeat seismicity had a dramatic influence on the tilt record during this time (section 4.5), but episodic cyclic tilt events were clearly recorded beneath the noise of the drumbeats. Station REM was installed in November 2005 and began immediately detecting tilt events which were temporally correlated with those at SEP, although the signal-to-noise ratio remained low on both stations through the early spring of 2006 and few well-correlated episodic tilt events were clearly seen until March 2006. By May 2006, the two stations showed nearly perfect correlation in the 30 s to 8 h band (Figure 4). After REM was destroyed by a large rockfall in May 2006 (see *Moran et al.* [2008b] for more about this event), SEP operated independently until late June 2006, during which time it continued to record clear, sawtooth-shaped episodic tilt events. Station NDM was installed in late June 2006 and recorded events which were very strongly correlated with

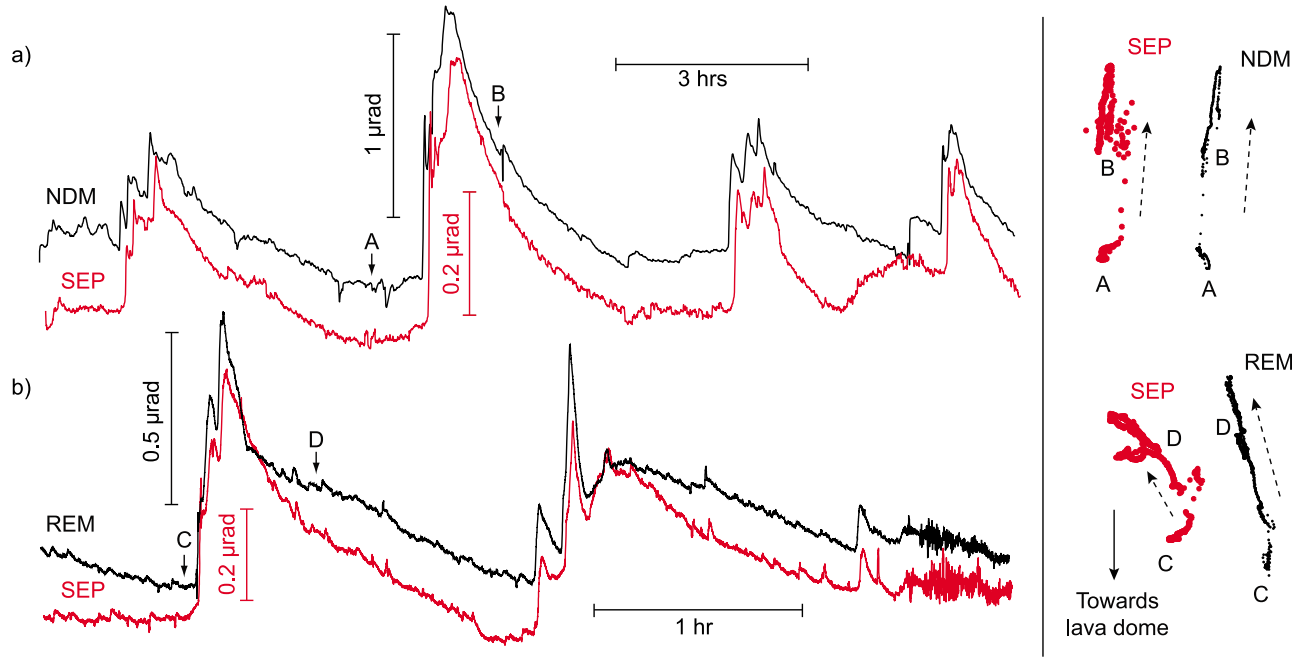

Figure 4. (left) Correlated, recoverable, asymmetric tilts resolved along the radial direction from the south edge of the 1980s dome to the tiltmeter (see Figure 1b). Data are filtered with a passband between 30 s and 8 h, and offsets and spikes are removed. In both pairs of time series, SEP is scaled in amplitude to match the other station, so separate scale bars are provided for each; time series are also slightly offset for clarity. (a) Tilt at NDM and SEP on 7–8 July 2006. (b) Tilt at SEP and REM on 9–10 May 2006. (right) Tilt vectors for each time series, showing generally unidirectional outward and inward tilts along a roughly constant tilt azimuth. Station SEP displayed more complex behavior than the other stations. Dots are plotted at equal time intervals, so dot spacing is inversely proportional to tilt rate. Letters A, B, C, and D show how the time series match the vector plots.

those at SEP (Figure 4) until SEP was destroyed in late 2006.

[19] More distant tiltmeters installed at Guacamole (GCP and GCL) and near the foot of the 1980s lava dome at GLA did not detect any clear episodic ground tilt during the eruption, nor did any of the Plate Boundary Observatory tiltmeters on the flanks of the volcano during the time that they were fully operational; the data from the PBO stations will not be addressed further here. Episodic tilts continued to be recorded at NDM until the end of the eruption in January 2008 (see section 4.6).

4.1. Tilt Cycles

[20] To examine episodic tilt cycles, we typically band-pass filtered the data between 30 s and 8 h (all data discussed herein can be assumed to be filtered in this way unless otherwise noted). For much of the eruption, a typical tilt cycle consisted of a rapid tilt away from the vent (outward tilt) over a period of minutes followed by a more gradual recovery in the opposite direction (inward tilt) over a period of minutes to hours (Figure 4). Cycles which began with inward rather than outward tilts also occurred, but were far less common. Many of the large tilt events also included a period of smaller-amplitude oscillatory behavior near the tilt maximum. Smaller and larger tilt events often piggy-backed on top of one another. Inward tilts often occurred at a gradually decaying rate, giving them a quasi-exponential appearance and the cycles a sawtooth-like shape. Most events at MSH were recoverable; that is, the final tilt roughly equaled the initial tilt (after removal of long-period trends of >8 h). We identified and recorded thousands of events in order to build statistics; details are given in section 4.4.

[21] Correlated tilt signals on SEP and REM were typically <1 μrad in amplitude (Figure 5). Amplitudes at NDM were often between 1 and 2 μrad early in the eruption, and increased in amplitude as the eruption progressed until by fall 2007 many events exceeded 4 μrad (Figure 5).

[22] Because of the large amplitudes and high signal-to-noise ratio recorded at NDM late in the eruption, tilt cycles were particularly well-expressed during this time (Figure 6). Defining the lowest point of outward tilt between adjacent peaks as the beginning of a tilt cycle, a typical cycle at NDM during December 2007 progressed as follows: (1) gradual tilt away from the vent over a period of hours at a slowly increasing rate, (2) sudden acceleration of tilt to rates sometimes exceeding 0.4 μrad/min, continuing for minutes (and sometimes associated with bursts of small VT earthquakes, see section 4.5), (3) often, a period of oscillatory behavior at the tilt peak, and (4) an inward tilt back toward the vent at an initially rapid but smoothly decaying rate, eventually transitioning to an outward tilt and the beginning of another cycle. Such behavior is consistent with cyclic tilt events detected earlier in the eruption at NDM, SEP, and REM, although at a larger amplitude.

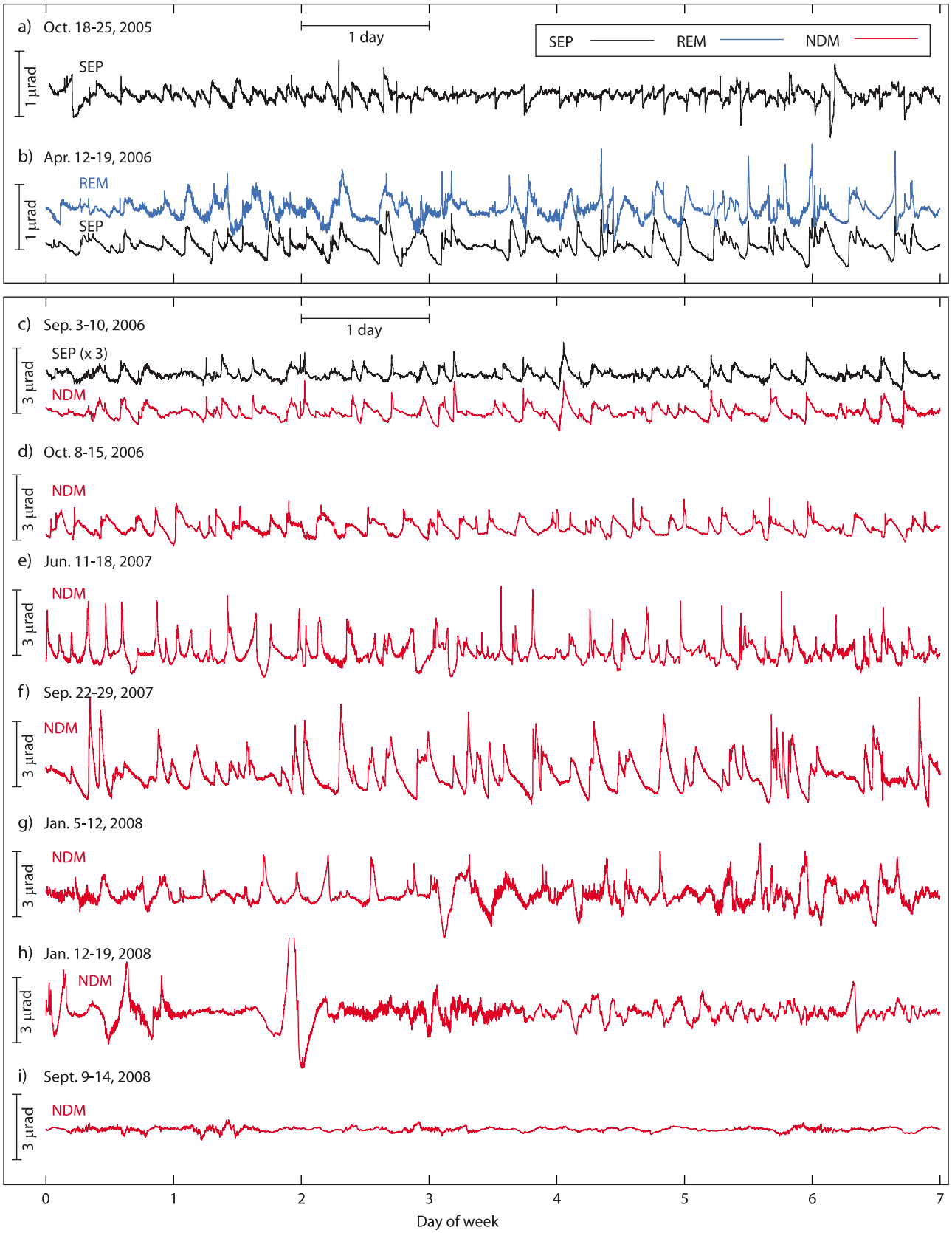
a) Oct. 18-25, 2005
1 day
SEP
REM
NDM
1 µrad
SEP
b) Apr. 12-19, 2006
REM
1 µrad
SEP
c) Sep. 3-10, 2006
1 day
SEP (x 3)
3 µrad
NDM
d) Oct. 8-15, 2006
NDM
3 µrad
e) Jun. 11-18, 2007
NDM
3 µrad
f) Sep. 22-29, 2007
NDM
3 µrad
g) Jan. 5-12, 2008
NDM
3 µrad
h) Jan. 12-19, 2008
NDM
3 µrad
i) Sept. 9-14, 2008
NDM
3 µrad
0
1
2
3
4
5
6
7
Day of week

Figure 5

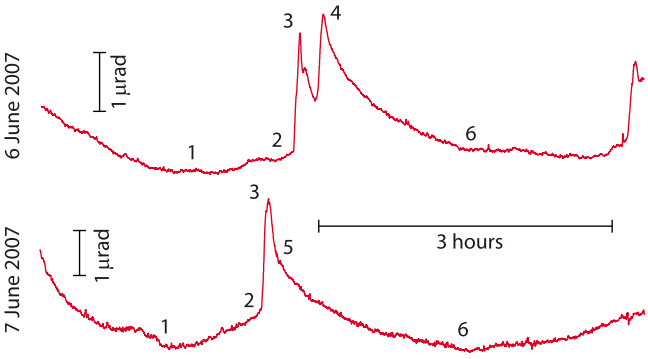

Figure 6. Example of large, clear tilt cycles during summer 2007 at NDM. Radial tilt shown. (1) Onset of gradual outward tilt; (2) onset of high-rate outward tilt; (3) end of high-rate outward tilt; (4) end of oscillatory behavior; (5) end of high-rate inward tilt; and (6) end of tilt cycle.

4.2. Vector Motion

[23] Plotting x tilt versus y tilt (we call these "tilt vector" or "particle tilt" plots), with each dot representing the tilt at a particular instant in time, shows that outward tilts associated with the beginning of tilt cycles usually occurred along a single dominant azimuth, while subsequent inward tilts usually occurred along roughly the opposite azimuth, although at a reduced rate (Figure 4). Such behavior produces lines of x-y tilt points in this type of plot, and we term this behavior "linearly polarized." Tilts were particularly polarized at REM and NDM, while SEP exhibited significantly more wander. The linearity of the outward portion of the signal suggests that we may accurately characterize outward tilts by the tilt amplitude and azimuth.

4.3. Correlation Between Stations

[24] To quantify the temporal correlation of ground tilt between stations, we rotated the data into a roughly source-radial coordinate system, with an origin centered on the south edge of the 1980s lava dome (see cross in Figure 1b). Correlation coefficients of radial tilt between stations SEP and REM during May 2006, over periods from minutes to hours, often exceeded 0.9 and in some cases even exceeded 0.98. Even very small characteristics of the tilt signals were often duplicated on both stations, demonstrating a very high signal-to-noise ratio in the data over these short time periods (Figure 4b).

[25] Correlation between SEP and NDM was similarly high, with correlation coefficients often exceeding 0.9. Although the signal at NDM was substantially larger than at SEP, the time histories of the signals were nearly identical (Figure 4a). We find agreement for tilts as small as 0.02 μrad (measured at SEP), both during episodic tilt cycles and between cycles.

4.4. Picked Events

[26] We implemented a simple algorithm to automatically pick high-rate outward tilts from the data. The algorithm identifies onset and cessation times of high-rate tilt events using strongly low-pass-filtered data (with a 20 min cutoff), but calculates amplitudes, azimuths, and durations using relatively unfiltered data so that the magnitudes of the episodic tilt events are not lost. At NDM, the autopicker identified more than 3,000 tilt events over the course of the eruption. Visual inspection reveals that the autopicker generally does a good job identifying high-rate tilt events, although events with smaller signal-to-noise ratios or very short durations are missed, start and end times of events are not always accurately identified, and some false picks are recorded.

[27] For increased accuracy and to verify the results of the autopicker, we also hand picked more than 1200 episodic tilt events from spring and summer 2006 at NDM, SEP, and REM. For each tilt event we hand picked the time and x and y tilt values for the following points: onset of gradual outward tilt, transition to high-rate outward tilt, end of high-rate outward tilt, end of oscillatory behavior associated with the tilt maximum, end of high-rate inward tilt, and end of all inward tilt (see Figure 6). Most events do not display all these features, but we picked those points that could be identified. We find that results for the high-rate outward portion of the tilt events are generally consistent with autopicked results.

[28] It it important to note that hand picking a limited number of points from a complex tilt cycle is not without significant uncertainty. Because inward tilts often featured a gradually decreasing rate that merged into background noise or other tilt cycles, and because smaller tilt cycles were often piggybacked on top of larger cycles, it was often very difficult to choose an end point for a tilt cycle. Since we picked only nonoverlapping events, smaller events piggybacked on larger events were not counted, which creates biases in event count, durations, and amplitudes. We also note that the high-pass filter used (4 h versus 8 h, for example) can have a strong effect on the apparent duration of precursory outward tilts, or the long tail of inward tilt. Finally, by picking only episodic tilt cycles with a rapid outward phase we necessarily neglect different types of tilt cycles that may be present.

4.4.1. Tilt Azimuths

[29] Figure 7 shows observed high-rate outward tilt azimuths for hand-picked events during summer 2006, and

Figure 5. Selected weekly time series from 2005 to 2008 at SEP, REM, and NDM. (a and b) Note that the first 2 weeks have a vertical scale that differs by 3 × from (c–i) the remaining weeks. In October 2005, SEP shows small, irregular tilt behavior, but by April 2006 the tilt events were larger, clearer, and correlated well with REM. Time series in Figure 5c show excellent correlation between SEP (with amplitude scaled up by 3 times) and NDM. Figures 5d–5i show evolution of NDM time series throughout the eruption. Note increasing amplitude of episodic tilt events as eruption progresses. Time series in Figures 5g and 5h show two sequential weeks near the end of the eruption; note cessation of regular episodic tilt events. Time series in Figure 5i shows activity at NDM approximately 8 months after the end of the eruption; episodic events are completely absent. All data were high-pass filtered with an 8 h cutoff.

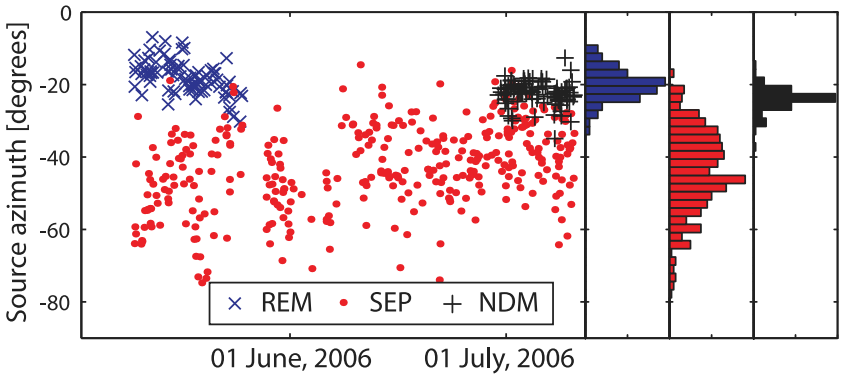

Figure 7. Hand-picked outward tilt azimuths during summer 2006. Azimuths are shown in local tiltmeter coordinates (relative to the tiltmeters' x and y channels rather than east and north).

Figure 8b shows autopicked outward tilt azimuths at NDM through the end of the eruption. Outward tilt azimuths remained remarkably consistent over the course of the eruption, although some wander did occur. It is not clear if this wander was related to changes in eruptive processes or to other effects, but the change in apparent azimuth around November 2006 does correspond to a jump in daily tilt rate (see section 4.4.3). Unfortunately, a data gap around this time makes more careful examination of this change impossible.

[30] As the histograms show, SEP exhibited considerably more variability than the other stations, which we believe may be due to instability in the local site. (This location also experiences significant thermal effects which may affect tiltmeter response, although we do not believe the thermal response to be important over the timescales of the episodic tilt events; see section A1.)

[31] Spatially, tilt azimuths recorded on the 1980s lava dome converged on a small area near the south edge of the dome (Figure 9) with little variation.

4.4.2. Tilt Durations

[32] Determining the duration of a complete tilt cycle is difficult for the reasons noted above. We therefore calculated durations only for the high-rate portion of hand-picked tilt events (from points 2 to 3 in Figure 6). Figure 10 shows a histogram of these outward tilts for all stations. Most high-rate outward tilts lasted between 2 and 10 min, with a long-tailed distribution of events extending to well over 100 min. Since many brief events with a small signal-to-noise ratio were not picked, these results must be biased toward longer tilt events.

4.4.3. Tilt Amplitudes and Rates

[33] Visual inspection of the time series suggests that tilt events at NDM became larger as the eruption progressed (see Figure 5). To quantify this observation, we examined changes in the amplitude of the autopicked high-rate tilt events over time, as well as changes in daily tilt rate (total outward radial tilt per day). Of course all conclusions drawn from the autopicked events are subject to the caveats associated with using the autopicker, and it is important to remember that small tilt events are much more difficult to detect than fewer large events although both could represent the same total tilt rate.

[34] Figure 8c shows high-rate tilt amplitudes at NDM. The great majority of events were <4 μrad, with a peak in events at around ~1 μrad, but the falloff in small magnitude events is at least partly due to picking biases and instrument noise. There does seem to be an apparent increase in the size of events following November 2006.

[35] We calculated daily radial tilt at NDM, exclusive of days with significant data gaps, offsets, or other artifacts. Figure 8d shows that from July to about November 2006, daily tilt rates at NDM averaged around 5 μrad/d, and only rarely exceeded 10μrad/d. Around November 2006, however, rates increased to 10–15 μrad/d and some days exceeded 20 μrad, while daily variation also seemed to increase. The higher tilt rate held largely constant (with several exceptions such as an apparent decrease in daily tilt rate around April 2007), until the final days of the eruption, when tilt rates became highly variable and finally dropped to zero for the first time.

4.5. Association With Seismicity

[36] A clear correlation between tilt and seismicity has been well documented at Montserrat [*Voight et al.*, 1998], where different portions of the tilt cycles correlated with increased levels of seismicity. As noted by *Iverson et al.* [2006], the 2004–2008 eruption of Mount St. Helens also offers an exceptional opportunity to link shallow volcanic seismicity with extrusion dynamics. However, the bulk of such analysis is beyond the scope of this paper, and here we summarize only key observations with the caveat that some of these observations may be superseded by future work.

4.5.1. LF and Hybrid Earthquakes

[37] Seismicity accompanying dome growth was characterized by LF and hybrid earthquakes and included (but was certainly not limited to) remarkable "drumbeat" activity as noted previously. Drumbeats occurred roughly every 1 min during the early part of the eruption, but repeat times increased and drumbeats nearly vanished by August 2005. They reappeared in October 2005 (close to the time of the first tiltmeter installation) with a recurrence interval of about 70 s [*Moran et al.*, 2008a], but became less common through 2006, and in 2007 were too irregularly spaced to warrant the term drumbeat (although they shared many other characteristics of the drumbeats) (S. Moran, personal communication, 2009). Finally, a small number of drumbeats

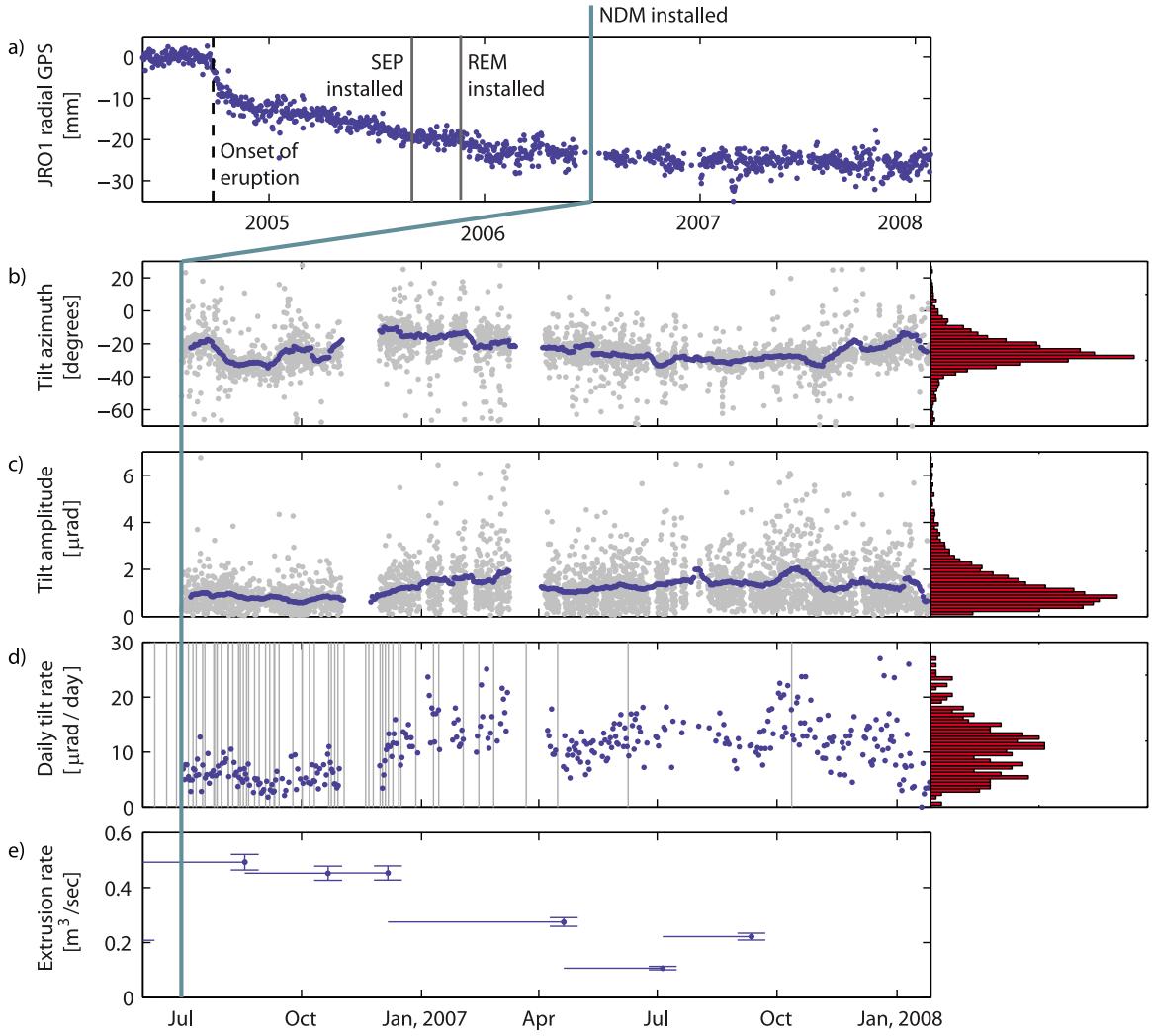

Figure 8. Evolution of geophysical signals during the 2004–2008 eruption of Mount St. Helens. Dark blue points in Figures 8b and 8c are 14 day moving averages. (a) Radial horizontal GPS time series at station JRO1, located 9 km north of the crater. (b) Apparent tilt azimuth for individual autopicked tilt events at NDM, in local tiltmeter coordinates. (c) Radial tilt amplitude of individual autopicked tilt events at NDM. (d) Daily radial outward tilt at NDM. Vertical gray bars represent M > 3 earthquakes from the Pacific Northwest Seismic Network database. (e) Extrusion rate, estimated by differencing subsequent estimates of dome volume (S. Schilling, personal communication, 2010). Error bars are shown only for the end of the time period between two dome volume estimates but are valid along the whole time period represented by the horizontal bars. Extrusion rate after September 2007 is poorly constrained, and not shown.

were associated with the very end of the eruption in 2008 (S. Moran, personal communication, 2009).

[38] Individual LF and hybrid earthquakes were often recorded on the Pinnacle tiltmeters as clear offsets or transient spikes in the data (Figure 11a). At SEP, spikes which occurred in association with drumbeat seismicity usually lasted for <8 s (which was usually comparable to the duration of most intense seismic shaking), occurred along generally elliptical vectors (outward tilt azimuth did not equal return tilt azimuth), and did not usually result in any permanent offset or change in the underlying tilt record. We believe these spikes to be mostly related to instrument response to seismic shaking, such as bubble motion, and not real ground tilt. Such behavior was not observed with the LILY tiltmeters.

[39] One of the motivations for installation of the tiltmeter network at MSH was to determine if the drumbeat seismicity was associated with episodic ground tilt (possibly related to lurching of the solid plug in the conduit [*Iverson et al.*, 2006]). However, tilt transients associated with the LF and hybrid events could not be identified, and the episodic tilt cycles which are the focus of this work exhibited little clear relationship with the LF and hybrid events (Figure 11b). We examined tilt data from December 2005 and found that in a few cases different parts of the episodic tilt cycle appeared

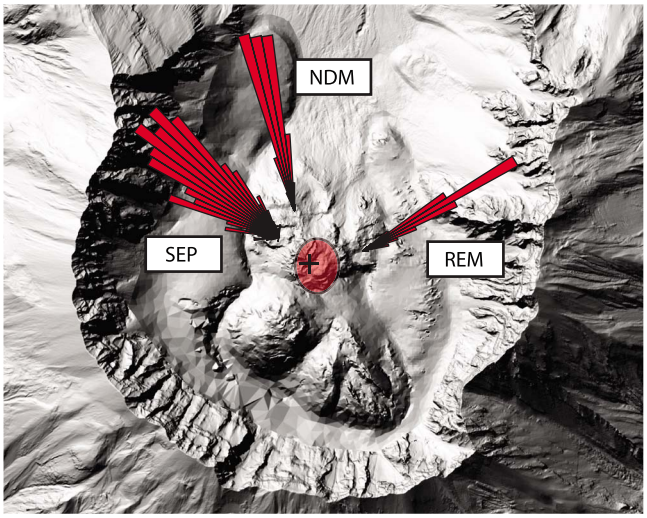

Figure 9. Rose plots of hand-picked tilt azimuths. Azimuths converge near the south end of the 1980s lava dome. Red oval shows approximate location of 1980 conduit, estimated from the location of a welt which grew on the crater floor following the 1980 eruption and was later buried by a series of lava domes. Black cross shows the location of the center of the radial coordinate system. Background shaded relief map is from February 2006.

to be correlated with some changes in drumbeat activity, e.g., reduced drumbeat activity during inward tilts, but in general, little correlation was apparent. As typical drumbeat periods were much shorter than typical episodic tilt cycles, and drumbeat activity declined dramatically throughout the eruption while episodic tilt activity did not, we conclude that the two processes are at most only indirectly related.

4.5.2. M > 2 Earthquakes

[40] Larger earthquakes of magnitude >2.0 also occurred during the eruption (Figure 8d shows M > 3 earthquakes from summer 2006 through the end of the eruption). These

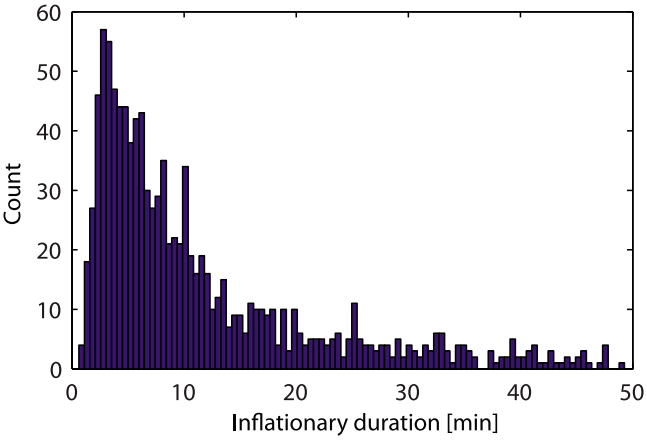

Figure 10. Duration of high-rate outward tilts for all stations, all time periods. Values greater than 50 min are excluded for clarity. Only the high-rate portion of outward tilts is shown; full tilt cycles were much longer.

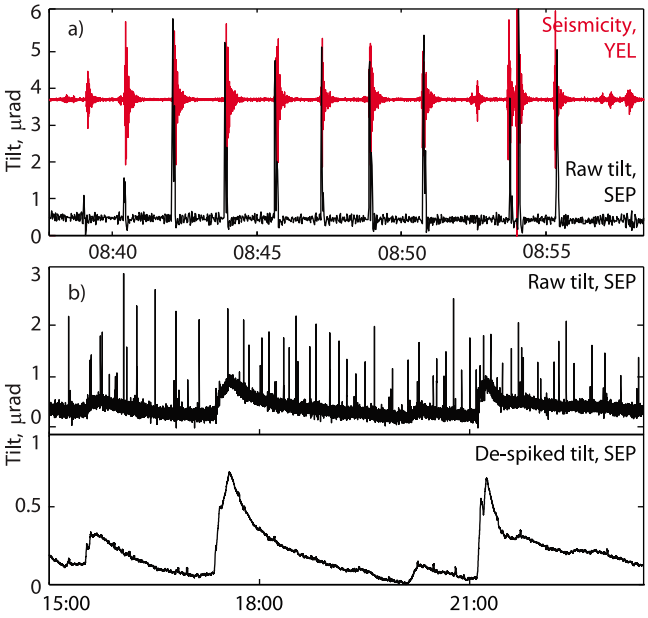

Figure 11. Earthquakes, tilt spikes, and episodic tilt. (a) Spikes in y channel of tiltmeter SEP and drumbeat seismicity at seismic station YEL on 1 November 2005. Tiltmeter clock adjusted to match more accurate seismic clock. (b) (top) North channel of raw tilt data showing earthquake-associated spikes on 11 December 2005. (bottom) After despiking and smoothing, underlying episodic events are clear. Y axis rescaled. Note difference in timescale between Figures 11a and 11b.

events shared several characteristics with the drumbeats including an LF or hybrid nature and tendency to exhibit down first motions on most seismic stations. They may have been related to lurching of the active spine, and may have occurred at the boundary between the base of the spine and the 1980s crater floor [*Moran et al.*, 2008a].

[41] These large earthquakes were recorded on Pinnacle tiltmeters as transients with durations roughly equaling the time of seismic shaking, or as permanent offsets (Figures 12a and 12b) which were easily distinguished from episodic tilt events. They were likely due to some combination of instrument response to seismic shaking and also real ground tilt. *Bonaccorso et al.* [1999] observed unreliable coseismic behavior on tiltmeters, and concluded that tilt offsets were due to instrument problems associated with the self-leveling motors. However, LILY instruments at Mount St. Helens (which did not appear to be as sensitive to seismic shaking as Pinnacle instruments), showed permanent offsets during some of these events, which suggests that some of the coseismic tilt may have been real.

4.5.3. VT Earthquakes

[42] With the exception of the onset of the eruption, there were many fewer VT earthquakes than LF and hybrid earthquakes at MSH. These VT events often occurred in bursts, were so small that they were generally recorded only on seismometers installed within the crater, and did not occur with regular temporal spacing like the drumbeats (S. Moran, personal communication, 2009).

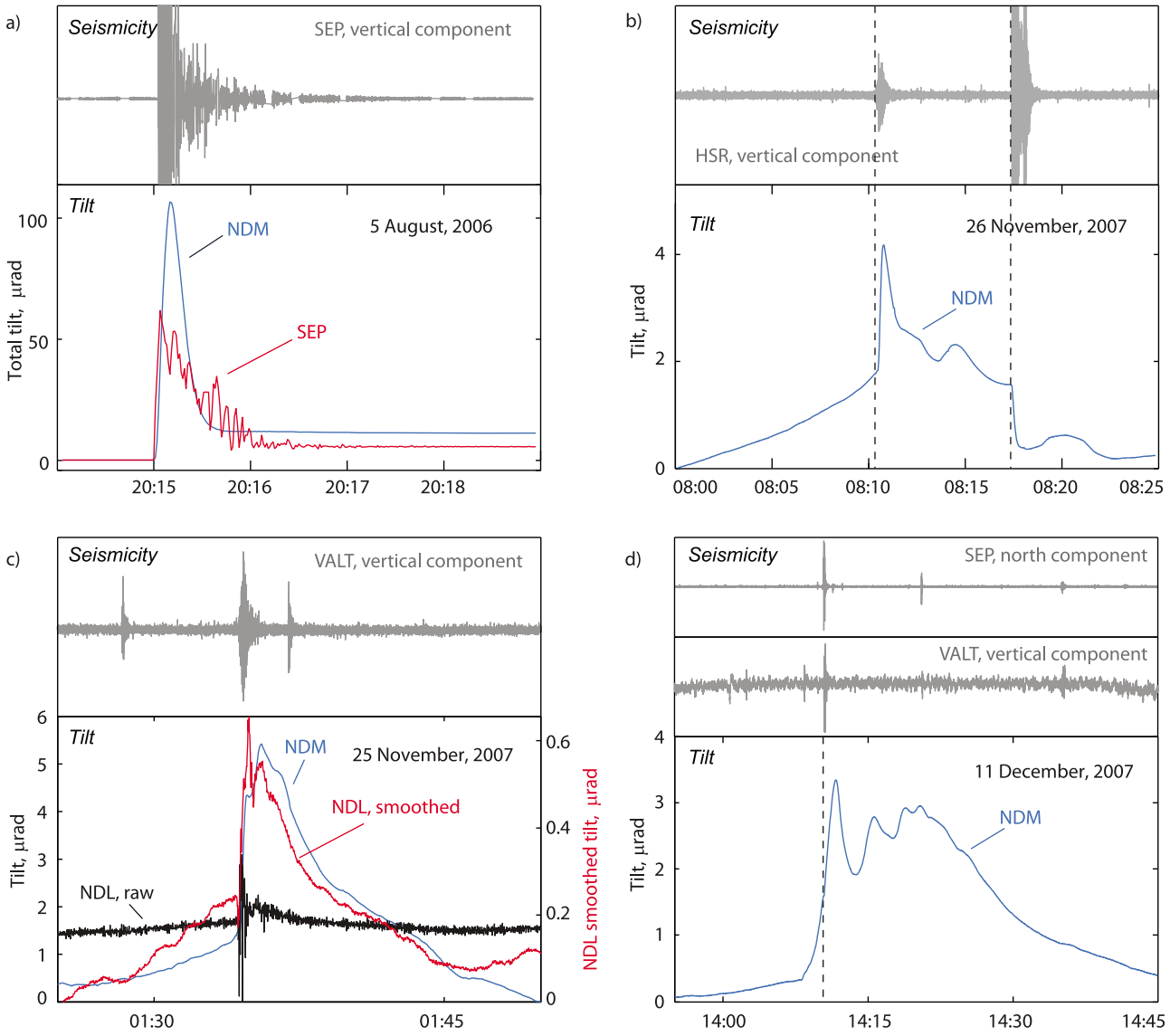

Figure 12. Examples of seismicity and tilt. (a) Effect of M 3.6 earthquake on tilt, 5 August 2006. Total tilt magnitude is shown, referenced to the first point. Seismic traces have been shifted to match tiltmeter time (which may differ substantially due to clock drift). NDM and SEP show large transients during the shaking, as well as permanent offsets. (b) Seismicity (vertical channel, station HSR) and episodic tilt (radial channel) at North Dome, 26 November 2007, showing either a small rockfall or VT earthquake associated with high-rate outward tilt, followed by M 2.0 long-period earthquake associated with a permanent offset in the tilt data. (c) Seismicity (vertical channel) and episodic tilt (radial channel) at North Dome, 25 November 2007, showing an earthquake (possibly a rockfall) associated with high-rate outward tilt. Seismic data are from broadband station VALT, located north of the crater. NDM response is typical of these events throughout the eruption, consisting of a high-rate outward tilt followed by gradual inward tilt. Raw NDL data show oscillations associated with the earthquake, followed by a small episodic tilt event, while filtered and normalized data agree fairly closely with NDM. Note different scale for filtered NDL data. (d) Rapid outward tilt associated with VT earthquakes on 11 December 2007. Vertical dashed line shows that the onset of high-rate outward radial tilt actually precedes the most intense seismic shaking caused by two small VT events, which show up clearly on seismic station SEP (located at September Lobe), although clock errors in the tilt data can make exact comparison difficult, and at least one smaller VT event occurred at around 1409 UT.

[43] VT earthquakes exhibited the most interesting correlation with episodic ground tilt at Mount St. Helens. Preliminary observations suggest that rapid outward tilts were often associated with either single VT events or bursts of VT events (Figures 12b and12d). However, tilt events also occurred in the absence of any detected seismicity, and occasionally in association with non-VT seismicity (Figure 12c). Analysis is complicated by extreme clock drift

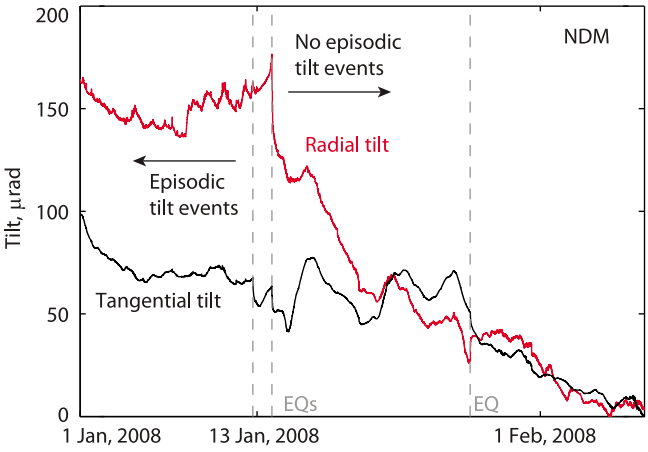

Figure 13. Tilt at NDM in early 2008. Large offsets in data are removed for clarity. Vertical gray bars indicate earthquake activity discussed in the text. Note cessation of visible episodic tilt after mid-January.

in the computer recording tilt data, which makes direct temporal correlation difficult, but we plan to more fully examine this relationship in future work.

4.5.4. Are Episodic Tilt Events an Artifact of Seismic Shaking?

[44] It is important to emphasize that while local seismicity did induce short transients in the tilt data, it seems clear that the episodic tilt events were due to real ground tilt and not instrument response to seismic shaking. Evidence includes the spatial correlation of tilt events, the fact that many episodic tilt events were not clearly associated with significant seismic shaking, and the onset of high-rate outward tilts which in some cases appeared to precede significant seismic shaking (Figure 12d). We also note that even $M > 2.0$ earthquakes typically caused tilt transients only during the actual seismic shaking, so there is no evidence that some sort of delayed tiltmeter response to seismic shaking caused the episodic tilt events.

4.6. Cessation of Eruption

[45] The cessation of the eruption provided important verification that cyclic tilt events were directly related to processes of volcanic extrusion. Episodic ground tilts occurred on the 1980s lava dome until January 2008. On the afternoon of 12 January (GMT),a period of seismicity was followed by a larger M 2.0 high-frequency earthquake and then several minutes of volcanic tremor. One day later, magnitude 2.9 and 2.7 earthquakes occurred along with a swarm of smaller events and associated tremor. Both the tremor and larger earthquakes introduced large offsets at both NDM and NDL. Finally, on 27 January another earthquake-associated tilt offset marked a substantial drop in seismicity at the volcano (S. Moran, personal communication, 2009).

[46] The clear, sawtooth-shaped tilt events which occurred throughout the eruption were not detected after the 12 January events (Figure 13), although some small-magnitude ground tilt probably related to volcanic activity continued until the 27 January event. Remote-camera photography verified the cessation of dome growth at around this time [*Cascades Volcano Observatory*, 2008].

5. Source Modeling

[47] To help constrain the location and mechanism of deformation, we invert the high-rate outward portion of a single "average" tilt event representative of tilt behavior from May to July 2006, when the tilt network on the 1980s lava dome was most complete. With the limited network of instruments we find that it is possible to fit the data reasonably well with many different types of simple source models, such as pressurized spheres, pressurized cylinders, and dislocations (or various combinations of these sources). Rather than searching for unconstrained best fitting simple models, we therefore consider only source models which we believe might plausibly produce the observed temporal evolution of the tilt cycles (rapid outward tilts and slow inward tilts), and we use the inversion results to attempt to falsify possible models and constrain source location and magnitude.

5.1. "Average" Tilt Event

[48] Tiltmeters only operated simultaneously at two of three sites on the 1980s lava dome where correlated ground tilt was detected. To invert for the source of deformation, we focus on the time period of May–July 2006, when the tilt network on the 1980s lava dome was most complete. We examined 86 tilt events seen simultaneously on stations REM and SEP during May, and 94 events seen simultaneously on stations SEP and NDM during July. Because no substantial qualitative or quantitative changes occurred in the tilt signals from May to July, and the tilt azimuths remained stable (see Figure 7), we assume that ground tilt during this period was generated by the same stationary source. We therefore use the data from all three tilt stations on the 1980s lava dome for inversion, despite the fact that at most only two of these stations were ever operating simultaneously.

[49] To calculate an average tilt event for inversion, we calculate the average outward tilt azimuth for each station, and calculate the average relative amplitude ratio between each pair of concurrently operational stations (Figure 14). Because station SEP operated during the entire time period, we can determine relative tilt amplitudes for all three stations on the 1980s lava dome. Additionally, we make the

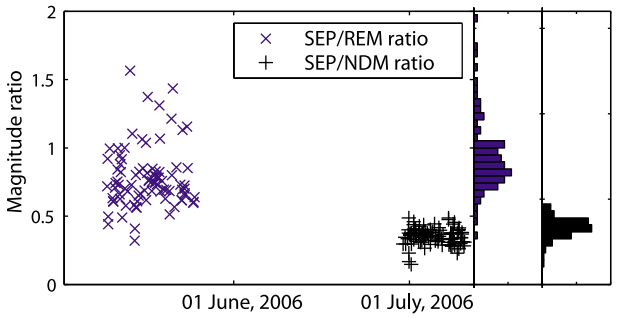

Figure 14. Ratio of tilt event magnitudes seen on the two sets of concurrently operating stations during summer 2006.

assumption of zero tilt for more distant stations, although these stations were not operational during the summer of 2006, because these stations did not record tilt at other times when it was detected on the 1980s dome.

[50] The assumption of a stationary source during summer 2006 allows us to average many events in order to reduce random background noise but not systematic biases such as those introduced by errors in installation orientation. With averaging, standard errors in the mean tilt azimuths were below 2° for all stations, but we cannot be confident that installation orientations are known to better than 10° for most stations (based on internal compass readings and additional field measurements, as well as analysis of teleseismic waves, see section A2). Uncertainty in station orientation thus dominates the uncertainty in tilt azimuth. For far-field sites GCP/GCL and GLA, which did not detect episodic events, we roughly estimate that we could have detected events of at least 0.02 μrad based on noise levels at these sites.

[51] Tilts of a wide range of amplitudes occurred at MSH but for inversion we choose a representative tilt of 0.2 μrad at SEP. For a representative event it is meaningless to calculate absolute uncertainties in tilt amplitudes; instead, because we calculate amplitudes at NDM and REM only relative to SEP, it is relative uncertainties that are important. We calculate the NDM/SEP amplitude ratio to be 2.83 ± 0.07 and the REM/SEP ratio to be 1.29 ± 0.04, where uncertainties are estimated using the standard error of the mean (these are probably minimum uncertainties). We set an uncertainty of 0.01 μrad at SEP, and using these ratios we construct an average tilt event with amplitudes at SEP, REM, and NDM of 0.20 ± 0.01, 0.26 ± 0.02, and 0.57 ± 0.04 μrad, respectively. However, as noted in Appendix A, anomalous behavior at the North Dome stations (most importantly, a difference in tilt azimuth and amplitudes at the two stations) suggests that uncertainties at NDM may be greater than indicated by the repeatability in the data. We increase the orientation uncertainty at this station to ±15° and increase the uncertainty in magnitude to 33% of the estimated magnitude (about 0.2 μrad for the modeled tilt event) to better reflect these uncertainties.

5.2. Calculation of Ground Tilt

[52] The rotation, or tilt, of any line segment depends upon the orientation of that line within the deformation field. Because a vertical borehole tiltmeter is narrow relative to its length and is oriented vertically, such an instrument is sensitive primarily to vertical gradients in horizontal displacements in the earth. The tilt of the instrument from vertical may be approximated for small displacement gradients as $\theta_r = \partial u_r/\partial z$, where u_r is displacement in any horizontal direction and z is the vertical coordinate. This expression requires knowledge of displacements at depth. However, we note that the shear strain ϵ_{rz} may be written as

$$\epsilon_{rz} = \frac{1}{2}\left(\frac{\partial u_z}{\partial r} + \frac{\partial u_r}{\partial z}\right), \tag{1}$$

and because stresses and therefore strains must vanish on the surface of a flat elastic half-space, $\epsilon_{rz} = 0$ and $\partial u_r/\partial z = -\partial u_z/\partial r$ (note that this is not generally true in the presence of topography [see *Meertens and Wahr*, 1986]). We may therefore compute tilt more conveniently as

$$\theta_r = -\partial u_z/\partial r. \tag{2}$$

With this expression we need only calculate vertical deformation on the surface of the half-space in order to calculate ground tilt. Appropriate analytical expressions exist for a number of sources.

5.3. Inversion Technique

[53] Inversions were performed using a Markov-Chain Monte Carlo method with the Metropolis-Hastings random walk [*Metropolis et al.*, 1953; *Hastings*, 1970]. We used uniform prior distributions for all unknowns, and constrained the source location to lie within a reasonable search volume in the crater. We assumed Gaussian data uncertainties and used the L_2 residual to calculate model misfit.

[54] The assumption of a flat elastic half-space allows the use of simple analytical ground deformation models. However, given the topography at Mount St. Helens (including the fact that distant, lower-elevation stations GLA, GCP, and GCL may actually be located below the source in some instances), the different rock types composing the 1980s dome and materials filling the crater, and the fact that the 1980s dome itself may be only partially coupled to the surrounding edifice, this assumption is certain to introduce unmodeled error into the inversions. We examined the first-order effect of topography on distant stations (which play an important role in constraining source depth) by constructing a simple radially symmetric finite element model of a shallow inflationary (Mogi) source beneath a lava dome in a uniform elastic medium. We find that for a shallow source 350 m below the surface (measured from the top of the dome) the deformation is concentrated within the lava dome itself, reducing surface deformation at the more distant stations relative to the homogeneous half-space. At 2 km from the dome, tilt is reduced by nearly an order of magnitude. For a deeper source at 1 km, however, we find that tilt at the distant stations is reduced by less than 10%. We conclude that topographic effects may significantly alter the response at distant stations for shallow sources, but probably do not significantly affect their ability to constrain deeper sources. Without more extensive modeling involving realistic topography derived from DEMs and more realistic laterally variable material properties, this effect is difficult to accurately characterize. We save such an approach for future modeling, and in this work assume a uniform elastic half-space.

[55] For the elevation of the half-space surface we use the average elevation of the three tiltmeters installed on the 1980s lava dome (2103 m). We use a shear modulus for the half-space of 1 GPa but acknowledge large uncertainty in this estimate: while the crater fill at Mount St. Helens almost certainly consists of weakly consolidated volcanic material with low shear modulus [e.g., *Chadwick et al.*, 1988], the 1980s lava dome itself consists of semifragmented dacite which may be considerably more rigid (although faults might reduce its effective rigidity).

[56] Data from five stations were used to constrain the inversions: three on the 1980s lava dome where volcanic tilt was detected (NDM, SEP, and REM) and two more distant

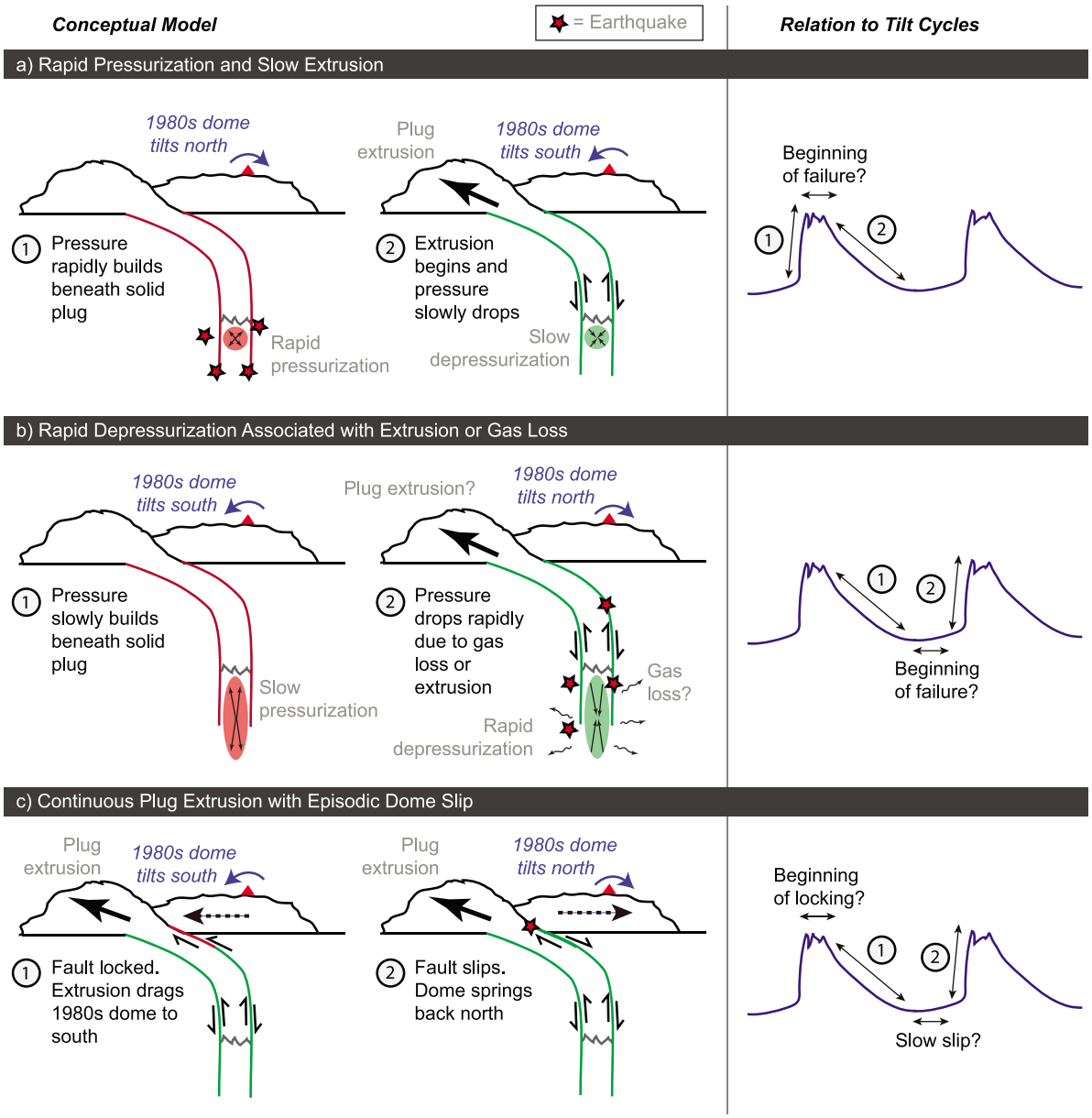

Figure 15. Three of the suggested models for tilt cycles at MSH (note that geometry is scaled differently from Figure 2 for clarity). (a) Rapid pressurization beneath the solid plug followed by episodic plug slip (section 5.4.1). (b) Rapid depressurization beneath the solid plug associated with either gas loss or plug slip (section 5.4.2). (c) Continuous extrusion with periodic locking and slip on the contact with the 1980s dome (section 5.4.3). For all models, red lines along the conduit indicate locking while green lines indicate slip, and corresponding points in tilt time series are shown on right.

stations where no tilt was detected (GLA and GCP). We also ran inversions using only the stations on the 1980s lava dome in order to evaluate the importance of the more distant stations, and found that these stations provide a valuable constraint on source depth (subject to the important caveats regarding topography noted above).

5.4. Models and Inversions

[57] Below we briefly motivate several possible source models which might plausibly explain the cyclic tilt signals observed at Mount St. Helens, including cyclic conduit pressurization and slip, conduit depressurization associated with slip or gas loss, continuous plug extrusion with episodic dome slip, an opening crack (associated with the hypothesized VLP source), and time-varying shear tractions on the walls of the conduit. For each proposed mechanism we identify an appropriate deformation source model and invert to evaluate the plausibility of the model as well as its characteristics (location, magnitude, etc.).

5.4.1. Rapid Pressurization and Slow Extrusion

[58] We first investigate models involving cycles of conduit pressurization/depressurization and plug extrusion or

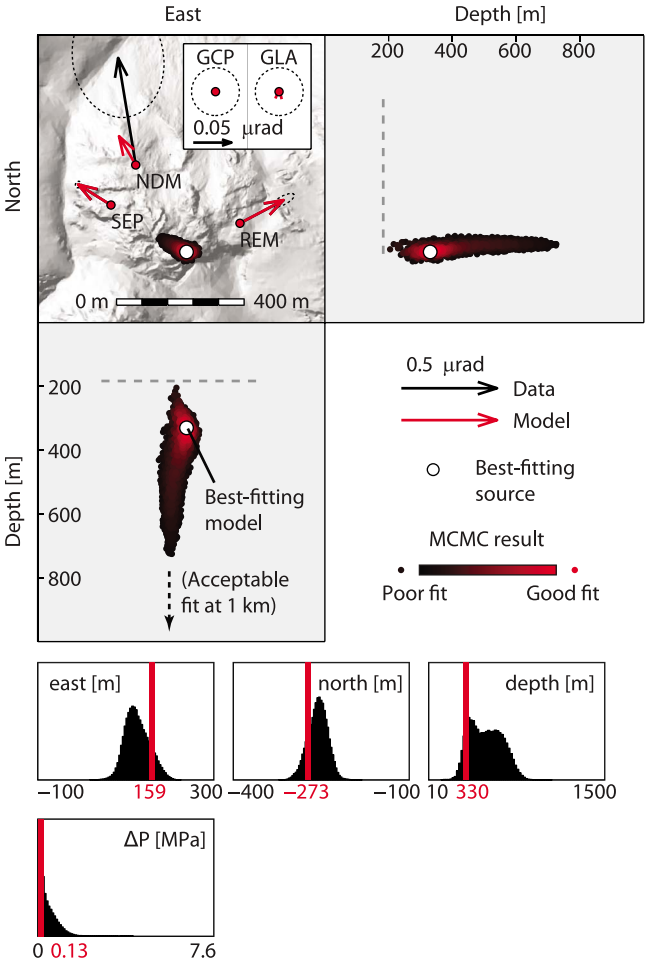

Figure 16. Monte Carlo inversions for isotropic pressure (Mogi) source. Inset shows fit to more distant stations GCP and GLA. Each point represents one of two million MCMC results, with points in the lowest 5% probability discarded; 95% confidence ellipses are shown. Dashed lines in cross sections indicate approximate depth to floor of old crater beneath the 1980s lava dome. Histograms show posterior probability distributions for modeled unknowns, with a vertical line indicating the best fitting model.

gas loss (Figure 15a). Intuitively, it might be expected that a model involving gradual source pressurization to some critical threshold followed by rapid depressurization (perhaps associated with gas loss or plug slip) would involve slow outward tilts and rapid inward tilts. Such behavior was clearly observed at Onikobe geyser in Japan where sawtooth-shaped tilt cycles recorded gradual outward tilts during pressurization and then rapid inward tilts associated with eruption of the geyser [*Nishimura et al.*, 2006] (at Montserrat, inward tilts were also generally more rapid than outward tilts [*Voight et al.*, 1999], although the cycles were more symmetric). This temporal behavior is, however, the opposite of that at Mount St. Helens, where rapid outward tilts and slow inward tilts were observed. We suggest two possible explanations for this paradox: (1) source pressure histories which, due to a complex interplay of nonlinear processes, involve rapid pressurizations and slow depressurizations and (2) vertically elongate source geometries which result in tilt sign reversals at certain distances from the conduit, such that rapid outward tilts are associated with source depressurization. We investigate the first possibility in this section and the second in section 5.4.2.

[59] Although cycles of rapid pressurization and slow depressurizations may be nonintuitive, recent work by *Lensky et al.* [2008] suggests that they may be possible. In this model, pressure in a conduit beneath a solid plug increases due to time-dependent gas exsolution, crystal growth, and influx of new melt from the chamber. When the pressure exceeds some limit the plug begins to slide with rate-dependent frictional behavior. As the plug slides, pressure beneath the plug drops, which leads to bubble expansion and an increase in permeability, which in turn increases gas loss. Pressure drops and the plug stops moving, leading to a new cycle. The complex interplay of these different processes can produce different types of cyclic behavior [see *Lensky et al.*, 2008, Figure 10], and given the many nonlinearities in gas loss, crystal growth, and fault friction, it seems plausible that that rapid pressurizations and slow slip events might occur.

[60] We have not attempted to model this process quantitatively at Mount St. Helens so this hypothesis remains untested. We speculate simply that rapid outward tilts might have occurred during conduit pressurization and slow inward tilts during slip of the plug and associated pressure reduction in the conduit. If the region of pressurization is relatively localized, it may be modeled using an isotropic pressure source. For an isotropic pressure source in an elastic half-space [*Mogi*, 1958] the expression for radial tilt θ_r at the surface of the half-space can be shown using equation (2) to be

$$\theta_r = \frac{3a^3\Delta P(1-\nu)}{\mu}\frac{rd}{R^5} \tag{3}$$

where a is the source radius, ΔP is the pressure change of the source, ν is Poisson's ratio, μ is the shear modulus of the half-space, r measures the radial source-receiver distance on the surface of the half-space, d is the positive source depth, and R is the total source-receiver distance $R = \sqrt{r^2 + d^2}$.

[61] With the exception of an underprediction of tilt at NDM, observed tilt is reasonably well modeled by an isotropic pressure source located beneath the south central part of the 1980s lava dome (see Figure 16, as well as the dashed line in Figure 1b for the approximate boundaries of the 1980s lava dome prior to growth of the crater glacier and the 2004–2008 eruption). The best fitting source depth of around 340 m is too shallow to be consistent with a model involving pressurization beneath a solid plug, but source depth is poorly constrained (see histograms in Figure 16). Inverting with a fixed source depth of 1 km results in an acceptable fit to the data. Residuals for both inversions are given in Table 2. Note that the deep model has a slightly better unweighted residual, but the weighted residual (χ^2) is higher due to the poor fit at SEP and REM (which have lower uncertainties).

[62] For a sphere with radius of 50 m the pressure change for the 1 km deep source is 3.5 MPa, which corresponds to a volume change of about 1400 m^3 (about 0.3% of the total volume). Scalar seismic moment may be estimated using

Table 2. Inversion Results[a]

Type	p	Depth (m)	Strength	$\sqrt{r^T r}$ (μrad)	χ^2	χ^2_{red}
Mogi	4	330	$M_w = -3.2$	0.41	7.2	1.2
Mogi (depth = 1 km)	3	1000	$M_w = -2.2$	0.38	36.1	5.2
Depressurizing conduit	5	700	$dP = -0.96$ MPa	0.85	1520	300
Dip-slip dislocation	7	260	$M_w = -2.1$	0.23	2.5	0.83
Dip-slip dislocation (<5 cm)	7	260	$M_w = -2.74$	0.39	6.5	2.2
Opening VLP crack	6	350	Opening = 1.5 cm	0.41	10	2.5
Conduit shear	5	200	$\tau = 3.1$ kPa	0.88	1490	299

[a]With p the number of fitting parameters and r the residual vector. The reduced chi-square metric is defined by $\chi^2_{red} = \chi^2/(n-p)$ where $\chi^2 = r^T\Sigma^{-1}r$ and n is the number of observations (here, 10). The opening sill is fixed to the location of the VLP source modeled by *Waite et al.* [2008], so has few free parameters. Depths for dislocation sources specify the bottom edge of the fault, and for the depressurizing conduit the depth is to the top of the source. Qualitatively, most of the models provide a similar fit to the data although residuals and χ^2_{red} values differ significantly.

$M_0 = 2\pi a^3 \Delta P(1-\nu)/(1-2\nu)$ [e.g., *Segall*, 2010]. Using $\nu = 0.3$, we obtain a seismic moment of 4.8×10^{12} N m, or a moment magnitude of $M_w = -2.2$.

[63] A possibly more realistic model involves pressurization of a significant vertical extent of the conduit. *Bonaccorso and Davis* [1999] derived an approximate expression for ground deformation due to a pressurized vertical pipe, and this was corrected by *Segall* [2010] for values of ν other than 1/4. Differentiating the vertical displacements using equation (2), we obtain

$$\theta_r = \frac{a^2 \Delta P}{4\mu}\left[\frac{r(1+2\nu)}{R^3} - \frac{3r^3}{R^5}\right]_{\xi=d_1}^{\xi=d_2} \tag{4}$$

where $R = \sqrt{r^2+\xi^2}$, ξ is an integration variable along the vertical coordinate, and d_2 and d_1 are the (positive) depths of the bottom and top of the conduit, respectively.

[64] We invert for this model assuming a conduit radius of 50 m, which is similar to that estimated for the 1980 eruption [*Scandone and Malone*, 1985; *Carey and Sigurdsson*, 1985], and consistent with an estimated vent radius of 50–100 m based on extruded spine dimensions during the 2004–2008 eruption [*Pallister et al.*, 2008]. We use a minimum pipe length of 500 m and a minimum depth of 700 m. We find that a deep pressurized pipe does not fit the observed tilt data at MSH, and we conclude that if there is a deep pressurizing source beneath the rigid plug during outward tilt, it must be relatively equant in shape (isotropic).

5.4.2. Rapid Depressurization Associated With Extrusion or Gas Loss

[65] Tilts due to vertical prolate ellipsoids undergo a sign change at some distance from the conduit such that a depressurizing source generates outward tilts at distances close to the vent. We invert for a depressurizing vertical prolate ellipsoid modeled using the solution of *Yang et al.* [1988]. This solution should provide results equivalent to those of *Bonaccorso and Davis* [1999] for very long slender ellipsoids but retains accuracy for less elongate shapes and allows us to more fully explore the range of aspect ratios which give rise to the observed tilts. Note that here we do not model the ground deformation generated by changing shear tractions on the walls of the conduit, which would occur if the rapid depressurizations were associated with plug slip.

[66] We find that a deep depressurizing source of plausible amplitude, shape, and location is capable of producing outward tilts on the 1980s lava dome which match the observed tilts reasonably well, but falsely predicts that inward tilts would have been observed at more distant sta-

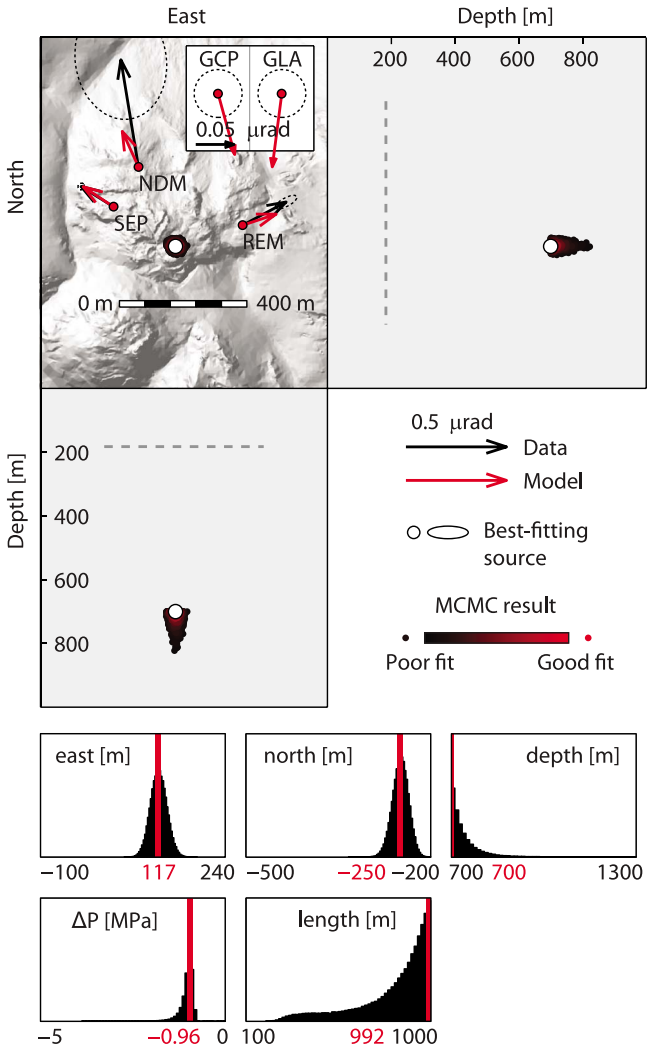

Figure 17. Monte Carlo inversions for a depressurizing vertical prolate ellipsoid located beneath the solid plug. See Figure 16 caption for more information. Dots from MCMC runs show the location of the top of the conduit (ellipsoid). Note that models shallower than 700 m are not accepted.

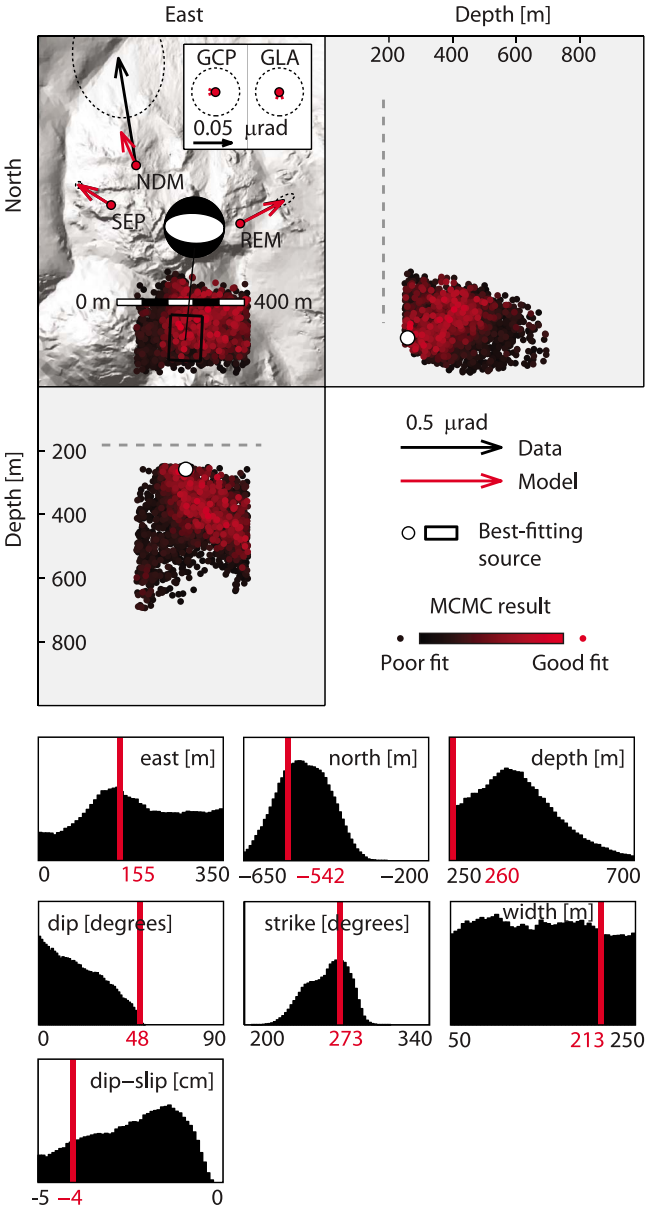

Figure 18. Monte Carlo inversions for slip on a normal fault located beneath the south part of the 1980s dome. See Figure 16 caption for more information. Dots from MCMC runs show location of the bottom center of the dislocation.

tions GCP and GLA at roughly twice the noise levels at these stations (topographic effects may play an important role, however; see section 5.3). For a source with top at 700 m, the pressure change is approximately −1 MPa (Figure 17 and Table 2).

5.4.3. Continuous Extrusion and Episodic Dome Slip

[67] We next investigate a model involving continuous plug extrusion with episodic stick-slip cycles on the contact between the 1980s dome and the extruding plug (Figure 15c). In such a model, inward tilts would have occurred as the 1980s dome was slowly dragged (via frictional coupling) to the south by motion of the plug; sudden outward tilts would then have occurred as the fault slipped and the dome elastically rebounded to the north.

[68] Excepting changes in frictional properties with time, this model might predict that daily tilt rate (see section 4.4.3) should be directly proportional to plug velocity. To get a rough estimate of the upper limit of the magnitudes involved, we assume total fault locking during nonoutward portions of the tilt signal, that is, that the 1980s dome is completely coupled to the extruding plug except during outward tilts (when slip occurs on the fault). The extrusion rate during summer 2006 was at least 0.45 m^3/s (see Figure 8e), yielding a linear extrusion rate of 5 m/d assuming a conduit radius of 50 m. With roughly 5–10 tilt events per day, a maximum of 1 m of slip would occur per slip event. This is probably too much slip to have remained undetected by other means such as GPS receivers on the 1980s lava dome and time-lapse photography of the extruding plug (see section 6.1), assuming slip with this magnitude reached the surface, and suggests that fault locking was not complete and/or that a considerable amount of the extrusion was accommodated in permanent long-period tilt which we disregard. Therefore, this value can be considered only an extreme upper limit on tilt-associated slip.

[69] Assuming that the top surface of the inclined plug/dome interface (Figure 2) acted as a planar fault surface (in reality the surface must be curved), rapid outward tilts due to slip on this fault may be modeled by an elastic dislocation [e.g., *Okada*, 1985]. We invert for a dip-slip fault with width constrained to 100 m near the south edge of the 1980s lava dome. Results (Figure 18 and Table 2) suggest that dip-slip faults at this location can produce the recorded pattern and amplitude of ground tilt. (Note that Figure 18 seems to show the dislocation as located beneath the 2004–2008 dome, but this site is actually very close to the south edge of the subsequently buried 1980s lava dome as shown by the dotted line marking the edge of the 1980s dome in Figure 1b.) The best fitting fault slips ~39 cm, dips to the north at ~60°, and fits the data (including the larger tilts at NDM) very well. However, although this is less slip than predicted by the maximum-locking model discussed above, it is still probably too much slip to have remained undetected by other means. We therefore invert for a fault with slip constrained to <5 cm and still find reasonably good fits to the data: the best fitting model dips to the north at 50° and gives a χ^2 value of 6.5, whereas the large-slip model gives $\chi^2 = 1.3$ (the poorer fit is mostly due to the smaller tilt predicted at NDM).

[70] Calculating scalar seismic moment M_0 for the best fitting 5 cm slip model using $M_0 = \mu SA$, where S is the average slip and A is the area of slip, and assuming a shear modulus of 1 GPa, we find that $M_0 = 8.6 \times 10^{11}$ N m ($M_w = -2.7$).

5.4.4. Opening/Closing Crack and VLP Source

[71] We next investigate the possibility that the tilt was generated by a VLP source modeled by *Waite et al.* [2008]. As noted earlier, VLP events during the summer of 2005 were found to be consistent with the opening and closing of a sill-dike combination located below the SW edge of the 1980s lava dome. The source was also found to be consistent with a combination of a sill and radially expanding cylinder, and, to a lesser extent, with a single crack dipping north at 30°.

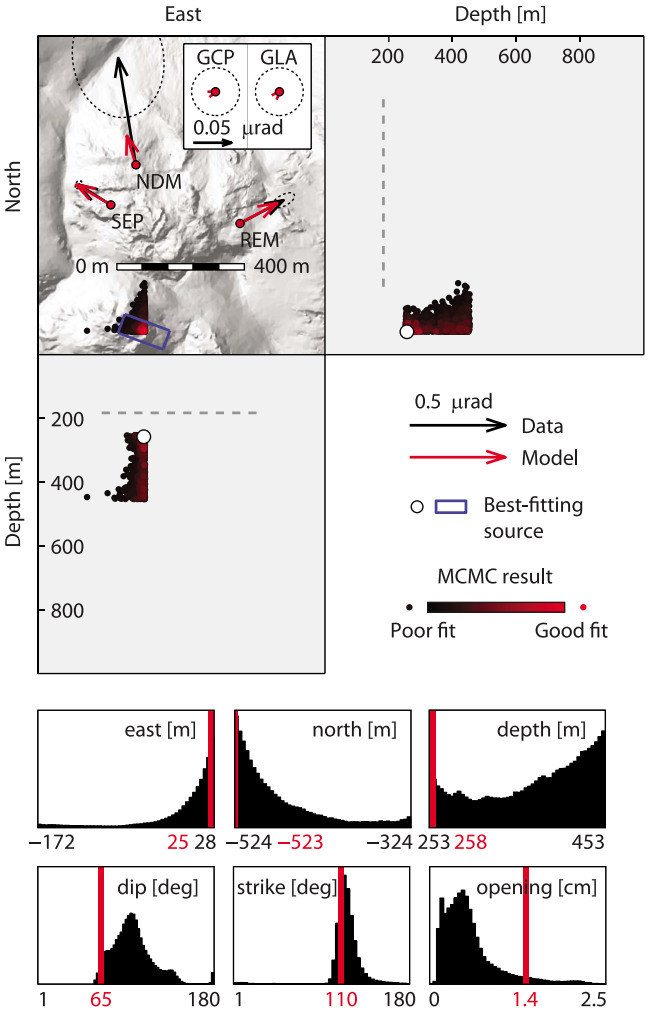

Figure 19. Monte Carlo inversions for an opening crack constrained to lie near the location of the best fitting VLP source of *Waite et al.* [2008]. See Figure 16 caption for more information. Dots from MCMC runs show location of center of dislocation. Abrupt edges to the cloud of accepted points are due to prior constraints on source location; opening models more to the east actually provide a somewhat better fit to the data.

[72] We invert to determine if a single opening crack in the location of the VLP source is consistent with the tilt data. We model a 150 m × 150 m crack constrained to lie within ±100 m laterally and vertically of the best fitting VLP source, and find that the tilt data can be fit reasonably well with a variety of steeply dipping opening cracks. The best fitting source strikes 110° and dips south at 65°, opening 1.5 cm (Figure 19), and we can fit the data nearly as well with a source dipping north at 103°, opening 0.5 cm.

[73] These models underpredict the tilt at NDM but correctly model the radial tilt pattern observed. The transient volume changes of the tilt and VLP sources are also similar: approximately ~300 m^3 for the tilt model and ~1000 m^3 in the deflating VLP sill, using the same shear modulus of 7 GPa. Differences in orientation between the best fitting tilt model and the single-crack VLP model may be attributable to topography (unmodeled in our inversion) or the different time periods of the data.

[74] Based on these results we cannot rule out the possibility that the tilt and VLP sources were closely related.

5.4.5. Variations in Extrusion Rate and Shear Tractions

[75] Shear tractions on the conduit walls exerted by moving magma or rock are understood to be an important source of ground deformation near the vent [*Green et al.*, 2006; *Chadwick et al.*, 1988; *Beauducel et al.*, 2000], but the effect is still poorly understood and is largely neglected during routine geodetic inversions. We investigate a model in which (unexplained) variations in conduit flow rate generate observed ground deformation at MSH by generating time-varying shear tractions on the conduit walls.

[76] We derived a simple analytical approximation for tilt due to a change in uniform shear tractions $\Delta\tau$ on the walls of a vertical cylindrical conduit embedded in an elastic halfspace (K. Anderson and P. Segall, manuscript in preparation, 2010). We find that integrating the vertical point force *Mindlin* [1936] Green's functions yields an approximate solution for constant vertical tractions on the boundary of the conduit, and using the finite element method we verified that this expression is accurate at large distances from the conduit relative to conduit radius. Tilt may be approximated as

$$\theta_r = -\frac{a\Delta\tau}{2\mu} r \left[\frac{\xi}{R^3} + \frac{(3-2\nu)}{R(\xi+R)} \right]_{\xi=d_1}^{\xi=d_2}. \quad (5)$$

[77] The best fitting horizontal source location is near the south edge of the 1980s lava dome. Inversions favor very shallow source depths and very short conduits, but we constrain the minimum depth to be 150 m and the minimum length to be 200 m. Conduit length is poorly constrained (Figure 20). For the best fitting model with a length of 210 m the change in shear tractions is 3.1 kPa, although this result scales with shear modulus and shorter conduits require greater tractions.

[78] This model underpredicts tilt at NDM, but explains the general amplitude and pattern of observed ground tilt. At such shallow depths, the magma at MSH is believed to be fully solidified; therefore, variations in shear tractions might be due to rate-dependent changes in sliding friction between the plug and the walls of the conduit. Unfortunately, the necessary parameters are so poorly constrained in this region that rate-and-state-dependent frictional theory cannot easily be used to check the plausibility of this model. However, we note that at 300 m depth the modeled change in shear traction is probably less than 0.1% of the lithostatic pressure.

5.4.6. Other Models

[79] It is worth noting that we have not considered deformation within the plug itself (caused by a bending of the conduit beneath the 1980s lava dome and suggested by Reidel shears in breccia and cataclasite in dome rock [*Cashman et al.*, 2008]), although such processes might generate surface deformation if they cause changes in tractions in the conduit. It also seems possible that frictional slip occurred at the margins of the plug at different times, such that slip on one part of the plug then would have led to outward tilt, while slip elsewhere would have led to inward

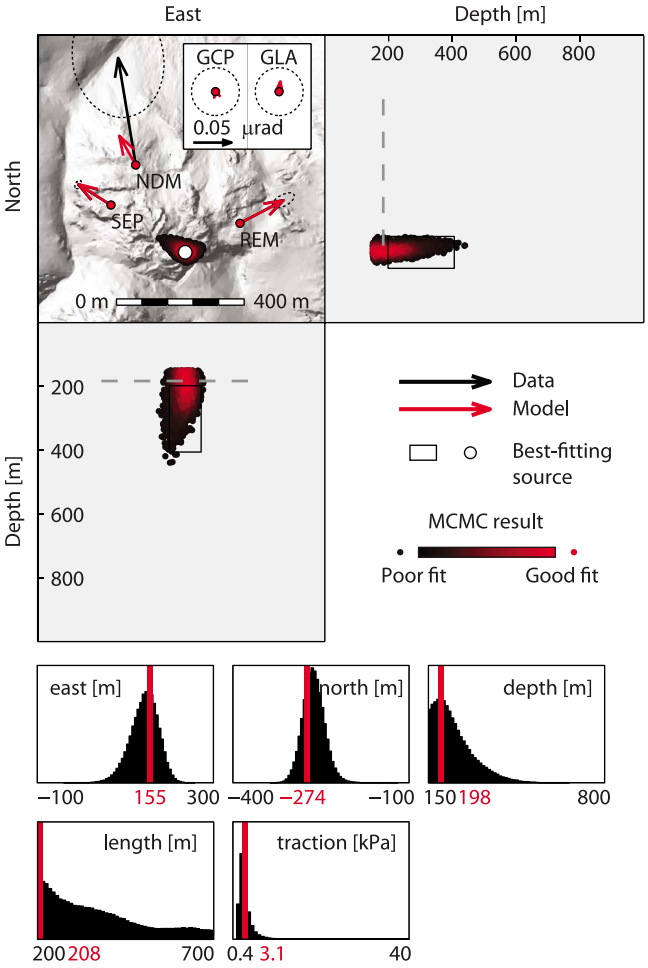

Figure 20. Monte Carlo inversions for conduit shear. See Figure 16 caption for more information.

tilt. However, we do not attempt to model these processes in this work.

6. Discussion

[80] At the least, a successful source model must be able to explain the pattern and magnitude of observed high-rate outward tilts, temporal evolution of the tilt events, remarkable constancy of tilt behavior (excepting an increase in tilt rate) over the course of the eruption despite changes in the rate of surface extrusion, and correlation with VT seismicity (although we defer most questions regarding the association between tilt events and seismicity to future work). Constraints from other observations may provide additional clues to help rule out unsuitable models, and below we consider some of these constraints.

6.1. Continuous Versus Episodic Extrusion

[81] Detailed knowledge of extrusion rates could help to distinguish between models predicting continuous extrusion and models predicting episodic extrusion. At Montserrat, for example, tilt deflations were correlated with increased rockfall activity, suggesting episodic spine extrusion during these times [*Voight et al.*, 1998].

[82] L1 GPS receivers operated on the 1980s dome during some of the same time periods as tiltmeters, and also operated on the growing 2004–2008 lava dome [*LaHusen et al.*, 2008; *Dzurisin et al.*, 2008]. High-rate (10 s) processing of the data shows steady extrusion, but noise levels are high and small-scale episodic displacements cannot be ruled out.

[83] Digital cameras were deployed for short periods of time near the vent at MSH to capture high-resolution, small field-of-view images of the active spine extrusion in order to measure extrusion rates and attempt to capture any stick-slip behavior (theorized to be associated with drumbeat seismicity). Measured extrusion rates were nearly constant, and sequences of images taken on 20 September 2005 showed no evidence of stick-slip motion greater than about 10 mm, despite drumbeat seismicity occurring every 2–3 min at the time [*Dzurisin et al.*, 2008]. Based on simple slip budget arguments, 10 mm is probably too large to eliminate the possibility of drumbeat-associated slip [*Dzurisin et al.*, 2008], but may provide a useful constraint for slip associated with episodic tilt events. Unfortunately, the tilt data from 20 September 2005 are heavily influenced by seismic shaking, and consequently, it is difficult to isolate episodic tilt events during this time. We see what appear to be episodic events during September, but during the time period of interest on 20 September there is only a single possible tilt event. Therefore, we are not confident of our ability to apply the 10 mm maximum-slip limitation to the tilt data. (Note also that the slip measurements only constrain motion at the surface, not at depth.)

6.2. Tilt Amplitudes and Physical Plausibility

[84] The magnitude of pressure changes estimated for some of the models might in principle be used to discriminate them from shear traction models. At Montserrat, tilt amplitudes would have required either very large source overpressures (possibly exceeding the strength of the host rock) or else source dimensions much larger than the expected size of the conduit, leading *Green et al.* [2006] to suggest a model instead involving shear tractions applied by magma to the walls of the conduit. However, the same argument cannot be made about the much smaller episodic tilts observed at MSH, and while very long period tilts over weeks to months were much too large to be explained by a shallow pressure source of reasonable overpressure, it is not clear that the long-period tilt was actually related to the episodic source process or even that it was real (see Figure A4). Therefore it remains difficult to discriminate between pressure and shear traction models at Mount St. Helens.

6.3. Tilt Rate and Extrusion Rate

[85] Most of the models examined above would seem to predict that a declining extrusion rate would lead to a decrease in daily tilt rate. Although it is very difficult to accurately estimate extrusion rates, which can only be interpolated from infrequent estimates of dome volume, from summer 2006 until September 2007 the extrusion rate appears to have dropped by roughly a factor of two, from ~0.4–0.5 m^3/s to ~0.2 m^3/s, based on dome volume estimates (S. Schilling, personal communication, 2010) (Figure 8e). However, tilt rates estimated in section 4.4.3 suggest a rough doubling of tilt rate during the same time period, from ~6.5 to ~11 μrad/d

(Figure 8d). These estimates are rough, but they do suggest that daily tilt increased while extrusion rates declined, opposite the result predicted by most simple models.

[86] Does this indicate a causal correlation between declining extrusion rates and increasing daily tilt rates? The answer it not entirely clear. Interestingly, seismicity at MSH did not appear to be correlated with variations in magma flux [*Moran et al.*, 2008a], suggesting a disconnect between these two processes. However, some correlation between extrusion and daily tilt rate is necessary, as the tilt rate dropped to zero at the same time extrusion stopped at the end of the eruption. If the decrease in extrusion rate was indeed causally related to the increase in tilt, then it is possible that the larger tilt rates represent an increase in the effective resistance of the shallow portion of the conduit. In this view, the evolution of the eruption was driven largely by the force balance between overpressure in the magma chamber and resistance in the shallow conduit (Figure 2). Since shallow conduit processes almost certainly include rate-and-state-dependent friction, volatile exsolution, gas loss, and other nonlinear processes, it is not difficult to imagine that shallow resistance might increase or decrease in complex ways. This increasing resistance would then have hastened (or even caused) the end of the eruption.

6.4. Fit to Data and Plausibility of Source Locations

[87] The locations of all the sources are consistent with upper conduit processes, with the exception of the VLP tilt source whose relationship to observable geological features is unclear. In map view, pressure and shear traction sources are located near the 1980s conduit as revealed in the 1980 eruption and subsequently buried by the 1980s lava domes (Figure 9). The depths of both the isotropic pressurization and the ellipsoidal (conduit) depressurization models are consistent with the base of the solid plug. The shallow best fitting isotropic pressure source is at a depth consistent with the solid plug itself, and while not compatible with the pressurization/depressurization models proposed here, it is not necessarily incompatible with other source models such as those involving deformation of the plug itself (although the mechanism of plug deformation would likely not resemble a simple pressure source).

[88] Dislocation models are consistent with the location of shallow extrusion beneath the south edge of the 1980s lava dome, near the site of initial phreatic explosions and the earliest extrusion during the eruption [*Vallance et al.*, 2008]. These models are also consistent with expected extrusion geometries (based on the transition from vertical conduit ascent to near-recumbent extrusion to the south of the 1980s lava dome), and patterns of seismicity from early in the eruption which suggest a conduit dipping at 45° to 60° northward at shallow depth beneath the old dome [*Thelen et al.*, 2008].

[89] Most of the models fit the average tilt vectors at SEP and REM and at more distant stations GLA and GCP to well within uncertainties, although the misfit at GLA is high for the depressurizing conduit model. Further discrimination between the models depends heavily on the uncertainty in estimated tilt at North Dome. Almost all models significantly under-predict tilt at this station, but unfortunately the uncertainties associated with tilt at NDM are difficult to quantify (see Appendix A) so the importance of this misfit is not clear. If the tilts and uncertainties we estimate for this station are accurate, then the inversion results support the large-slip dislocation inversions over the other models. However, because of the uncertainty in the NDM tilt and because all inversions use a simple elastic half-space assumption (which must certainly introduce significant biases into the results) we conclude that it is impossible to rule out any of the proposed models solely on their ability to fit the tilt vectors observed during summer 2006.

6.5. Other Constraints

[90] It is worth noting that the 2004–2008 eruption of Mount St. Helens was relatively gas poor (that is, depleted in excess volatiles [e.g., *Gerlach et al.*, 2008]). Degassing rates were low, and cycles of degassing were not observed (but not necessarily absent).

[91] Gas exsolution and possibly escape could play an important role in both the rapid pressurization and rapid depressurization models proposed above (sections 5.4.1 and 5.4.2, respectively). While the 2004–2008 eruption was relatively gas poor, vesicularity in the dome clearly indicates that bubbles did form in the upper conduit, and further work is required to determine if this volatile exsolution is compatible with the model developed by *Lensky et al.* [2008] for Montserrat or with models involving slow pressurization and rapid depressurization. We note, however, that the rapid depressurization model proposed here does not necessarily rely on volatile exsolution: pressurizations could also be caused by influx of new melt from below, and depressurizations by episodic plug slip.

[92] We save most analysis involving seismicity for future work, but at least to first order most of the models proposed here do seem plausibly capable of generating seismicity during rapid outward tilts (see red stars in Figure 15). Different models would produce different kinds of stress perturbations, which would be reflected in the seismic data, but unfortunately most of the recorded VT events were too small for focal mechanism solutions (S. Moran, personal communication, 2010). Different models would also produce earthquakes in different locations, so precise relocation of the tilt-associated earthquakes may provide important clues to source processes.

7. Conclusions

[93] Tiltmeter networks have the ability to record small, transient ground deformations which are otherwise difficult to detect, and can help to shed light on cyclic behavior at erupting volcanoes. While tiltmeter data are notoriously difficult to interpret, the diversity and extent of the tiltmeter network installed during the 2004–2008 eruption of Mount St. Helens, including both syneruptive and posteruptive periods, offers a unique opportunity to carefully examine and verify the behavior of tiltmeters in a volcanic environment. This work has underscored the importance of installing multiple instruments with good spatial coverage and also, if possible, utilizing colocated instruments for purposes of redundancy and data verification. We have also found unfiltered high-rate (1 Hz) data quite valuable, as it has allowed us to test instrument response using teleseismic and

microseismic waves, and allows for a closer examination of the correlations between local seismicity and ground tilt.

[94] While we do not believe that we see evidence of drumbeat-associated ground deformation at the volcano (one of the prime motivations for installing the tiltmeter network at Mount St. Helens), analysis is complicated by the erratic coseismic behavior of Pinnacle tiltmeters installed at MSH and we cannot completely rule out the possibility that small coseismic deformation did occur. Instead, we have discovered thousands of recoverable, episodic longer-period cyclic tilt events which went undetected by other instruments. These tilt events were detected on the 1980s lava dome during the eruption, typically exhibited rapid outward tilts followed by slower decaying inward tilts, showed high temporal correlation between instruments, and ceased at the end of the eruption.

[95] We propose several models to explain the temporal evolution of ground tilt at MSH and test them using simple deformation models which we compare to tilt data from summer 2006. These models include stick-slip behavior on the dome/plug margin, cycles of rapid pressurization and slow plug extrusion, cycles of slow pressurization and rapid depressurization, and an opening crack at the location of a VLP seismic source modeled by *Waite et al.* [2008]. Results consistently suggest a shallow tilt source located beneath the 1980s lava dome, closely associated with the 1980 eruptive conduit.

[96] We attempt to use additional constraints to help discriminate between models. The anticorrelation between tilt rate and extrusion rate suggests that models involving cycles of locking and slip on the plug-dome interface would require a change in coupling over time. We are unable to discriminate between the models on the basis of tilt amplitudes or observational constraints on stick-slip versus continuous extrusion. Source locations are consistent with known geologic structures such as the 1980s conduit or the dipping shallow conduit (with the possible exception of the VLP source). Source mechanisms seem plausibly capable of generating seismicity associated with rapid outward tilts.

[97] We conclude that the episodic tilt events at Mount St. Helens were generated by a shallow source located beneath the center to southern edge of the 1980s lava dome, and most likely associated with shallow conduit processes or possibly some sort of steam-filled crack. The episodic 1980s dome slip model is particularly appealing as it provides the best fit to the data and is consistent with well-developed fault gouge on the margin of the dome and with extrusion geometry at the volcano. We also favor the rapidly depressurizing conduit model for its conceptual simplicity (it does not rely on complex nonlinear interactions as with the rapid pressurization model), and because cycles of slow pressurization and rapid depressurization have been inferred at geysers and other volcanoes.

[98] Ultimately, however, the paucity of stations within the crater prevent discrimination between different source models based on the tilt data alone, and other observations such as extrusion rate or tilt amplitudes provide only modest additional constraints on tilt source. Further discrimination between source models will require additional work. In particular, we believe that a detailed examination of the intriguing relationship between tilt and VT seismicity at Mount St. Helens will be necessary in order to fully understand the nature of both these processes at the volcano.

Appendix A: Data Verification

[99] We verified and calibrated instrument response using teleseismic waves, microseismic noise, wind-associated ground tilt, diurnal ground tilt, very long period ground tilt (drift), episodic ground tilt, by physically rotating two of the instruments in their borehole, and through the installation of colocated instruments by different manufacturers. Tiltmeters by different manufacturers were colocated in two separate locations at Mount St. Helens: (1) at Guacamole, where a Pinnacle Series 5000 tiltmeter and a LILY tiltmeter were installed in separate boreholes approximately 6 m apart, and (2) at North Dome, where Pinnacle and LILY instruments were colocated in a single borehole (Pinnacle instrument NDM at ~2 m depth and LILY instrument NDL just below the surface). The use of different types of instruments provided a valuable check of data validity and improved our ability to separate instrument response from real ground tilt [e.g., *Mortensen and Hopkins*, 1987]. We also verified that episodic tilt response was not correlated with thermal effects or instrument supply voltage.

[100] Observations of anomalous behavior at the two North Dome stations motivated much of this analysis, although careful examination of tiltmeter data using a variety of signals is always prudent. While all of the Pinnacle instruments installed on the 1980s lava dome (including NDM) recorded similar episodic tilt events throughout the eruption, NDL recorded these events with a dramatically smaller amplitude or not at all (Figure A1). High-rate outward tilts were particularly absent at NDL, even while they were simultaneously being recorded at NDM, and vector plots indicate that the tilt direction at NDL wandered more than at the other tiltmeters.

[101] NDM and NDL operated concurrently during the eruption from only mid-November 2007 until January 2008, and then continued to operate together in the posteruptive period. To examine the different station responses, we studied 61 episodic tilt events at NDL. Because tilt cycles at NDL exhibited a far lower signal-to-noise ratio than at NDM, picking events was often difficult. We chose to examine inward rather than outward tilts at NDL as they often appeared more clearly, and we used the much stronger signal at NDM to help choose onset and cessation times. Inward tilt orientations at NDL averaged 177° ± 18°. Assuming that these inward tilts were reversals of the preceding outward tilts (as noted for the other stations on the 1980s lava dome), then inflations occurred at 357° ± 18°. At NDM, more than 180 outward tilts during the same time period averaged 336° ± 4°, a difference of ~21°. While the azimuths are therefore crudely consistent between instruments, we must still explain why the episodic tilt events appeared roughly 5–10 × smaller at NDL.

[102] The two stations also responded differently to coseismic shaking (section 4.5), recorded different very long period tilts, and recorded different tilts associated with wind. Last, tilt at NDM also showed an apparent preference for a particular azimuth, so it was important to verify that NDM was not recording tilt from only a single preferential direction due to instrument malfunction. In the following sections

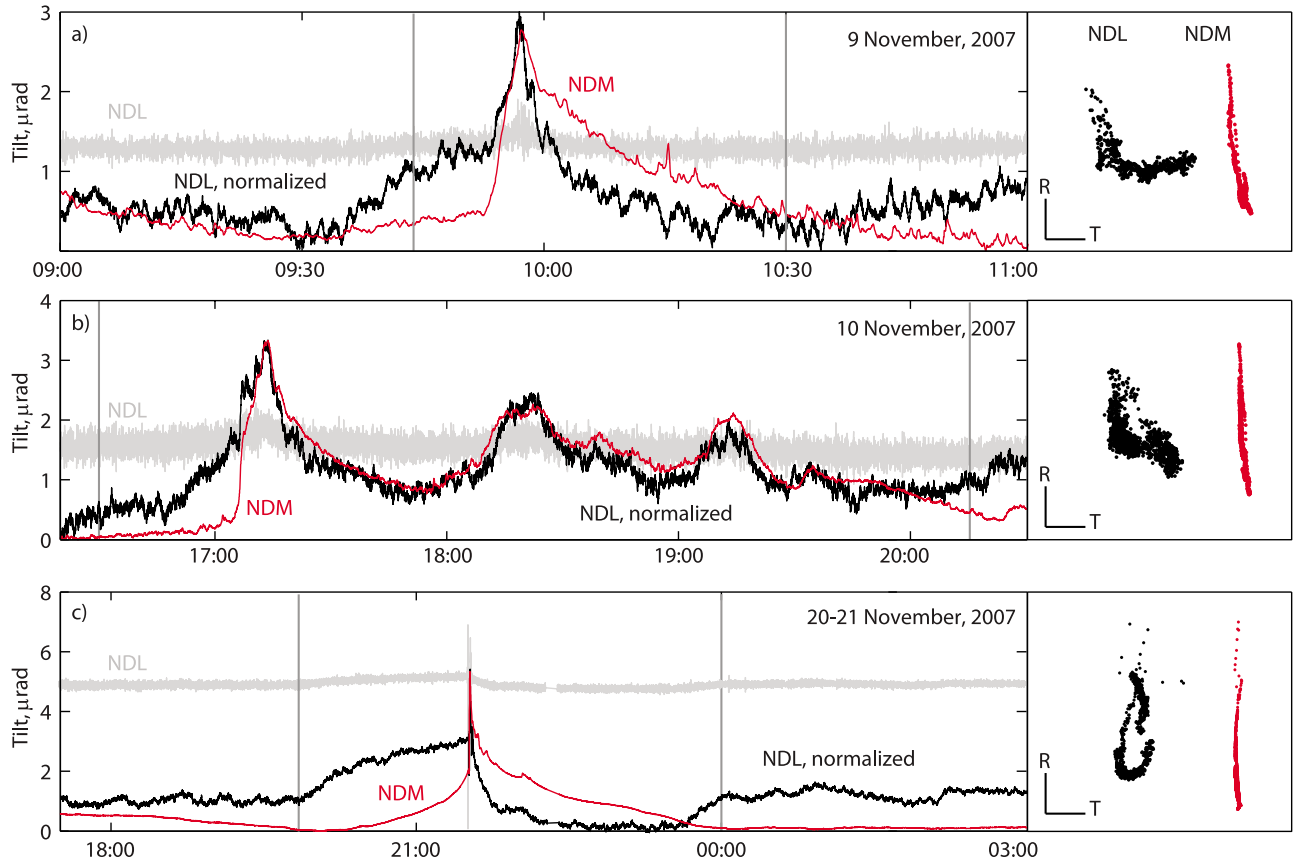

Figure A1. Comparison time series for radial tilt at NDM and NDL. Gray is NDL unfiltered and without normalization. Amplitude of episodic tilt at NDL is much lower than at NDM, but after filtering and normalizing the time series usually show reasonable agreement. Wind noise associated with storm systems is clear at NDL in Figures A1a and A1b. In Figure A1c, note that NDL begins to inflate around 2000 UT, at the same time as NDM, but high-rate outward tilt amplitude is lower. Normalized radial-tangential particle tilts are shown to the right of each time series; time range of particle plots are shown as vertical gray lines in the time series. Linear tilt polarization is extremely high for NDM and moderate to poor for NDL. See also Figure 12.

we discuss the analyses undertaken to further examine these apparent anomalies, as well as to verify the data from the tilt network as a whole.

A1. Correlation of Tilt with Temperature and Voltage

[103] Thermal changes result in both real and apparent ground tilt, the former due to thermally induced stresses in the ground and the latter due to thermal changes in the tiltmeter and borehole system. At Mount St. Helens, station SEP was located near significant hydrothermal activity and experienced particularly dramatic temperature changes of more than 50°C (at rates of up to 30° over just a few days) which make the station useful for examining thermal effects on tiltmeter performance and verifying that episodic tilts were not an artifact of thermal changes. Figure A2 shows tilt versus temperature over periods of 1 year, 1 week, and 1 day. While temperature changes strongly were correlated with recorded ground tilt over yearly and weekly time periods, they did not correlate with the episodic tilt events. For the longer time periods, correlations sometimes exceeded −20 μrad/°C but were highly variable with time and at different periods.

[104] Ultimately, it is impossible to fully separate the effect of real ground tilt from apparent ground tilt due to instrument effects; while the thermal response of the instrument's sensor should theoretically not exceed several μrad/°C [*Bonaccorso et al.*, 1999; *Wyatt et al.*, 1988; *Applied Geomechanics Inc.*, 2007], the tiltmeter + borehole combination may experience a much different thermal response (R. Krug, personal communication, 2010). To avoid these effects, we treat tilt data over any period longer than several days as suspect.

[105] Figure A2 also shows the changing voltage in the instrument's electronics due to battery charge-discharge cycles, and that these cycles did not correlate with episodic tilt events. We do note that at other times, however, many of the stations did record closely correlated voltages and temperatures, often with virtually no phase lag, despite the fact that temperature was recorded within the borehole while voltage changes were caused by sunlight striking the solar panels at the surface. This suggests a very rapid propagation

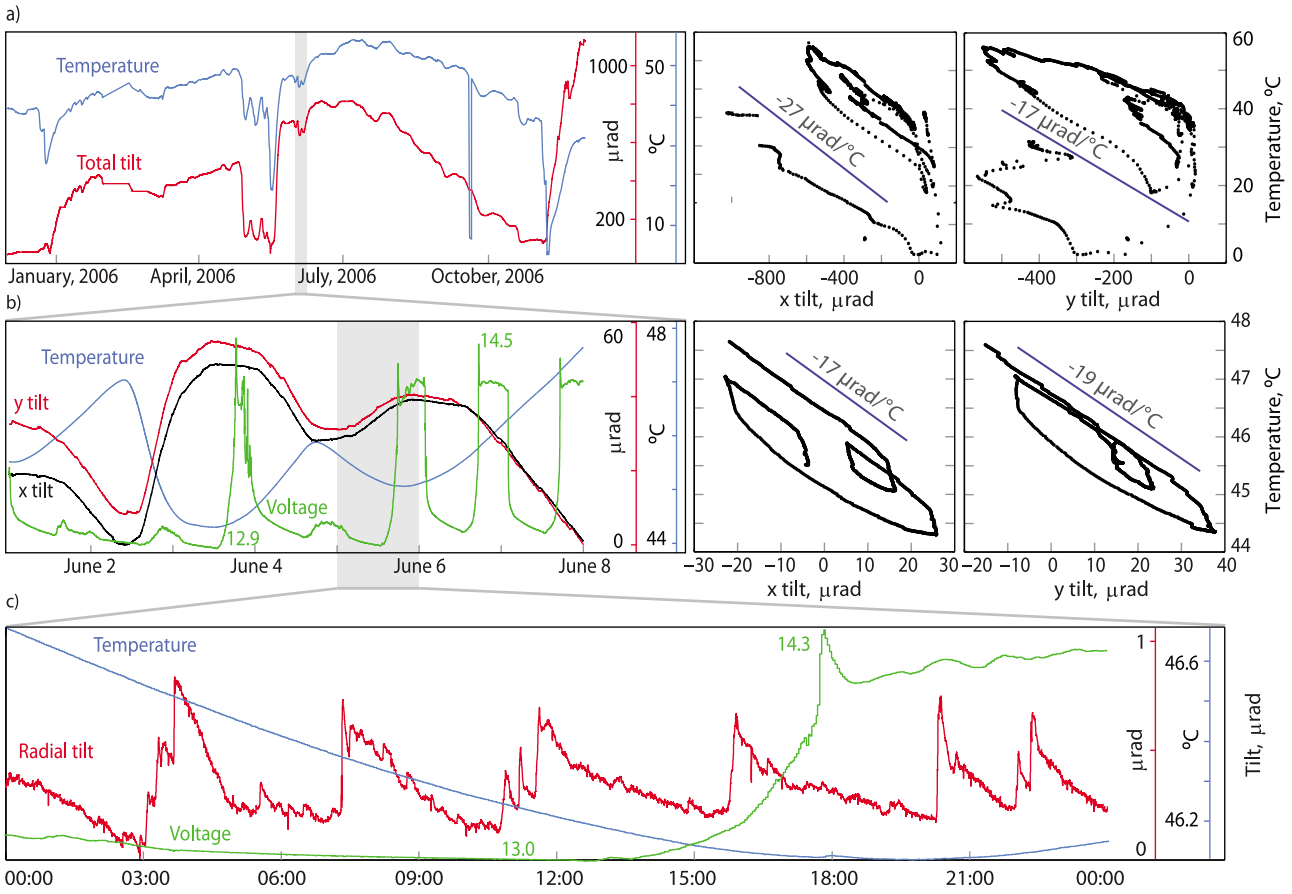

Figure A2. (left) Tilt, temperature, and voltage at SEP for 1 year, 1 week, and 1 day. Shaded boxes in time series show regions of enlargement below. (right) Scatterplots show correlations between tilt and voltage; diagonal lines show roughly approximated correlations coefficients, which change for different time periods. (a) One year. Note large temperature changes and correlated tilt magnitude (defined as $\theta_{mag} = \sqrt{\theta_x^2 + \theta_y^2}$, relative to the beginning of the displayed time series). (b) One week. The x tilt and y tilt are plotted, along with temperature and voltage. Tilt correlates with temperature but not voltage. Maximum and minimum voltages are indicated in the figure. (c) One day. Radial tilt (band-pass filtered between 30 s and 8 h), temperature, and voltage. Episodic tilts show no correlation with temperatures or voltages.

of temperature down the borehole, or possibly a voltage dependence in the temperature readings in the instrument electronics. In other cases, voltages and temperatures were also correlated with tilt recorded by the instrument; these tilts were most likely caused by thermal stresses generating real ground tilt (section A3).

A2. Teleseismic and Microseismic Waves

[106] Tiltmeters respond to both ground deformation and acceleration. For propagating waves the relative importance of these effects may be estimated by examining the ratio $g/\omega c$, where g is the acceleration due to gravity, ω is the frequency of the wave, and c is phase velocity [*Agnew*, 1986]. For a seismic wave traveling at several kilometers per second with a period of roughly 20 s, a tiltmeter will respond chiefly to accelerations. Therefore, teleseismic (as well as microseismic) waves provide a valuable check of tiltmeter electronics (such as gain settings) and orientation in the ground, but cannot confirm the instrument's response to actual quasi-static ground tilt.

[107] The tiltmeters at MSH all recorded clear teleseismic wave trains including P, S, and surface wave arrivals, although only surface waves and occasionally S waves appeared clearly on stations NDM, GCP, and GLA, which applied stronger low-pass filters to the data. Rayleigh waves typically appeared most strongly in the records, but interference with other waves complicated the recorded signals and made estimation of a tilt azimuth sometimes difficult.

[108] We rotated the tilt data into global N-E coordinates and directly compared the time series from different stations which shared similar internal filters (Figure A3). We found very good agreement, indicating that relative orientations were mostly correct and that instruments operated properly (we do note a small relative misalignment at Guacamole, with GCL = GCP + 20°, and perhaps a slight misalignment at North Dome, with NDL = NDM + 10°). We also compared measured and predicted Rayleigh Wave propa-

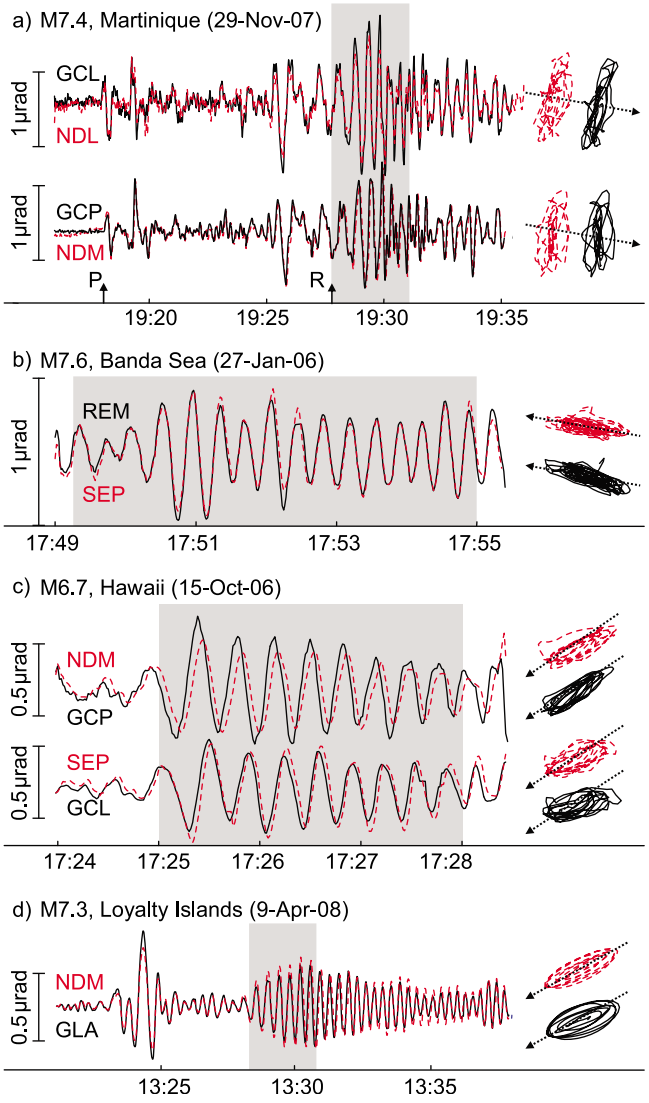

Figure A3. (left) Response of tiltmeters to four different teleseismic events. Time series show either north or east channels. (right) Particle tilt plots correspond to shaded regions in time series, and arrows show theoretical back azimuth toward the source. These predictions match particle motions closely, except for the Martinique event which probably reflects dominant Love rather than Rayleigh waves (perhaps due to coupling with topography). (a) Agreement between two LILY instruments (with a 6 s smoothing filter) and two Pinnacle instruments (plotted separately). Arrival of P waves and Rayleigh waves are marked with small vertical arrows, as determined from theoretical travel time calculations. (b) Excellent agreement between two "unfiltered" Pinnacle instruments. (c) Two filtered Pinnacle instruments, and an unfiltered Pinnacle instrument with a LILY instrument. (d) Two Pinnacle instruments.

gation directions for several large distant earthquakes. Averaged over a number of events we find mostly good agreement, confirming absolute tiltmeter orientations to within uncertainties.

[109] Microseismic noise can provide an additional check of instrument orientation and operation, at higher frequencies than teleseismic waves. Microseisms were observed on all stations, particularly during stormy winter months, and appeared at frequencies which are consistent with ambient seismic noise due to ocean waves and other processes (roughly 0.12 to 0.28 Hz) [e.g., *Aki and Richards*, 2002]. Microseismic noise was highly correlated between tiltmeters of similar type even over distances of several kilometers (Figure A4), and displayed lesser but still significant correlation between different types of instruments. Instruments without strong internal filters displayed similar amplitudes, while more strongly filtered instruments (NDM, GCP, and GLA) recorded amplitudes roughly an order of magnitude lower due to the filter. These results again confirm relative installation orientations for the tiltmeters as well as proper operation of the electronics.

A3. Diurnal and Semidiurnal Ground Tilt

[110] Earth and ocean tides may be used to check instrument response to ground tilt over periods of hours to days and can be used to calibrate instrument orientation [*Levine et al.*, 1989]. Short-base vertical tiltmeters should be deeply buried in order to record tides at a high signal-to-noise ratio [*Wyatt et al.*, 1982], but at MSH the tiltmeters were installed at shallow depth (due to the difficulties associated with installing tiltmeters on an erupting volcano using only helicopter support) where they were subject to thermally induced ground tilt and other effects.

[111] Diurnal tilts were clearly detected at several stations (NDM/NDL and REM) with amplitudes exceeding several microradians, and tilts were often strongly correlated with changes in voltage and temperature; these tilts were most likely caused by thermal stresses generating real ground tilt (while daily conductive temperature variations should only extend to roughly 1 m or less below the surface [*Bonaccorso et al.*, 1999; *Wyatt et al.*, 1988] they may create stresses which extend to greater depths, and may reach greater depths in highly fractured rock). The amplitudes were probably too large for solid earth or ocean tides, excepting very large amounts of topographic amplification (solid earth tides should be roughly 0.1 μrad [*Kohl and Levine*, 1993]), and at

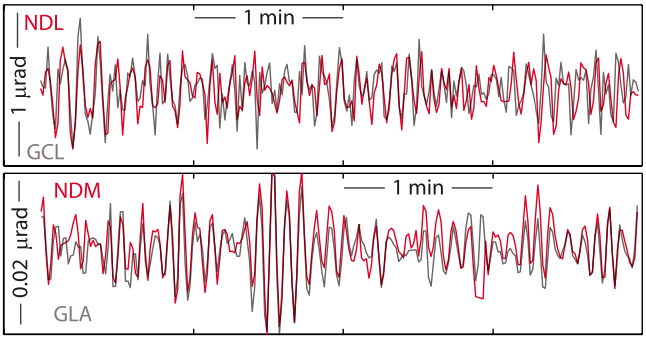

Figure A4. Microseismic noise. (top) LILY stations NDL and GCL on 17 November 2007. These stations were located more than 2 km apart but agree quite closely. (bottom) Pinnacle stations NDM and GLA on 20 April 2008. Note much smaller amplitude on Pinnacle stations, largely due to internal low-pass filter. North channels are shown, data high-pass filtered to 60 s.

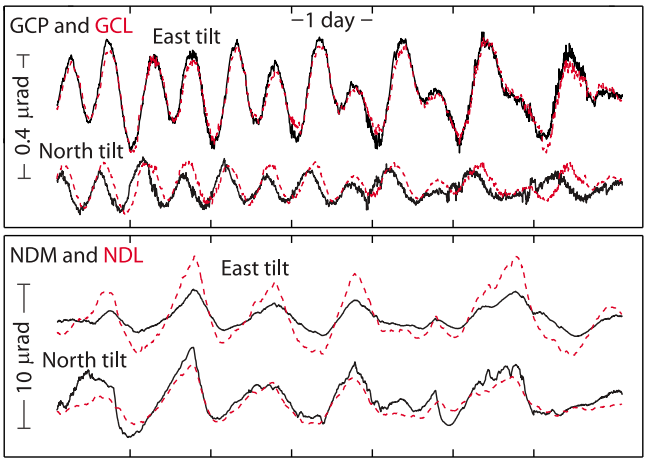

Figure A5. (top) Diurnal tilts at colocated station pairs at Guacamole from 29 August to 4 September 2007 (GCP, solid lines; GCL, dashed lines). (bottom) Diurnal tilts at North Dome from 4 March to 10 March 2008 (NDM, solid lines; NDL, dashed lines). Agreement is excellent at Guacamole and good at North Dome. Difference at North Dome is partly due to difference in apparent tilt azimuth between the two stations. Note much smaller amplitude at Guacamole, where stations were installed in deeper boreholes.

the distance of MSH from the coast the ocean tides should not be any larger [*Agnew*, 1986]).

[112] Diurnal and semidiurnal tilts were best recorded at colocated stations GCL and GCP, which were located several kilometers north of the crater and installed at a greater depth than the other instruments at MSH. These instruments recorded very similar ground tilt with peak amplitudes of roughly 0.5 μrad (Figure A5), allowing for a slight rotational misalignment (GCL = GCP + ~20°). Semidiurnal tilts have a similar character but slightly smaller amplitudes. Spectral analysis reveals clear diurnal phases K_1 and O_1 and semidiurnal phases M_2, S_2, and N_2.

[113] To compare colocated tiltmeters at North Dome, we examine posteruptive data. Band-pass filtering around the ~24 h diurnal cycle, we find that diurnal cycles agreed very closely, although with a rotational misalignment between stations of about 30° (NDL = NDM + ~30°). Diurnal cycle amplitudes often exceeded 5 μrad. This agreement, despite the fact that NDM was buried more deeply than NDL, suggests that diurnal stresses tilted the entire borehole. Band-pass filtering around the 12 h semidiurnal cycles we obtain similar results; although semidiurnal cycles were smaller in amplitude, they still often exceeded 1 to 2 μrad or more. Large semidiurnal tilts cannot be explained by thermal cycles, so this observation suggests that tidal ground tilt may play a role in generating semidiurnal (and presumably diurnal) tilts at MSH, with amplitudes perhaps enhanced by topographic coupling.

[114] Diurnal ground tilts rotated along with manual instrument rotation at NDM/NDL (see section A2), demonstrating that sensor response to thermal changes were not the primary driver of diurnal tilt cycles. On the other hand, the amplitude of both diurnal and semidiurnal tilts decreased noticeably at NDL but increased slightly at NDM after rotation, suggesting that coupling between the borehole and the instrument may have played an important role.

A4. Very Long Period Ground Tilt

[115] It is well known that continuous geodetic time series may display considerable wander over long time periods, although at short periods the error may be largely frequency-independent white noise [*Langbein and Johnson*, 1997]. Long-term trends recorded in tiltmeter data are a combination of real ground tilt (including localized tilt in the region of the borehole) at the site and instability in the instrument and installation [*Kohl and Levine*, 1993]. An examination of behavior on a tiltmeter network at Piñon Flat Observatory led *Wyatt et al.* [1988] to conclude that most long-period fluctuations were due to movement of near-surface material rather than instability of the instruments; this suggests that shallow instruments, no matter how well designed, may never properly record small, long-term tectonic tilt. On the other hand, it is worth noting that carefully designed tiltmeters (particularly long-baseline instruments) in deep boreholes or caves have shown long-term stability much better than 1 μrad/yr.

[116] None of the tiltmeters at MSH showed stability even beginning to approach 1 μrad/yr. All MSH stations drifted from tens to hundreds of microradians, led by NDM with more than 3000 μrad of tilt over the course of the eruption. While some of this drift is almost certainly due to real ground tilt associated with large-scale motion of the 1980s dome to the north (long-period azimuths at REM and NDM were generally consistent with GPS velocities suggesting motion of the 1980s lava dome to the north to accommodate emplacement of the new 2004–2008 lava dome [*LaHusen et al.*, 2008]), it seems clear that much was due to instrument or installation instability, or shallow local ground tilt. This conclusion is supported by the fact that colocated stations

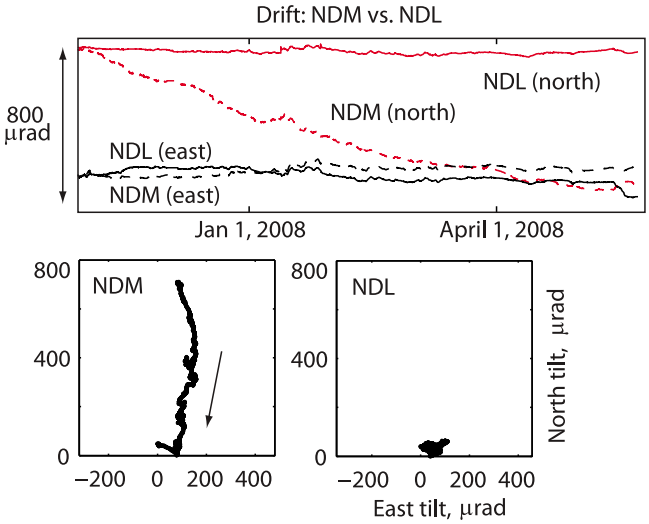

Figure A6. Differences in long-term drift at colocated stations NDM and NDL. (top) Time series at both stations. East channels are similar, but north channels differ by hundreds of μrad over 6 months. (bottom) Vector plots showing remarkable southward drift at NDM. Offsets are removed from the data.

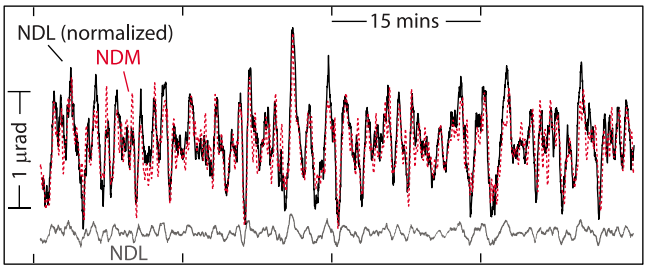

Figure A7. Correlation of wind noise at NDM and NDL for 23 March 2008. In global coordinates the dominant azimuth for wind-related ground shaking differed by nearly 90° at the two stations, and time series show no clear correlation. However, in local tiltmeter coordinates (shown) the time series happen to align very closely (with the data from NDL normalized). Correlation of y axes in local coordinates is shown. Both stations show strong linear polarization in the vector plots. Data band-pass filtered between 30 s and 10 min.

NDM/NDL and GCP/GCL displayed substantially different long-period tilt. From fall 2007 through spring 2008 NDM tilted over 600 μrad more to the south than NDL (Figure A6), yet after removing the long-term trend the stations agreed relatively closely for intermediate periods. Colocated stations GCP and GCL also displayed substantially different drift, with GCP drifting generally to the south over 7 months during the summer and fall of 2007 while GCL drifted north. Finally, we note that drift at SEP was clearly correlated with strong temperature changes of ~50° at the site (section A1).

[117] We conclude that long-period drift recorded on instruments at MSH was a complex mix of volcanic and nonvolcanic processes and cannot easily or reliably be used to draw conclusions about volcanic processes. This is in contrast to tilt at the volcano following the 1980 eruption, when tilts over periods of weeks to months of >2000 μrad and with rates that sometimes exceeded 300 μrad/d were used to successfully predict six effusive eruptions in 1981 and 1982 [*Dzurisin et al.*, 1983].

A5. Tilt Associated with Atmospheric Conditions (Wind)

[118] Periods of high background noise lasting from hours to days were commonly detected across the tiltmeter network; this noise often corresponded to shaking recorded on a broadband seismometer installed at Studebaker Ridge several kilometers northwest of the crater, as well as periods of high wind recorded at a weather station at Coldwater Ridge (reported by the Northwest Weather and Avalanche Center). This wind-associated ground tilt has been detected at every one of the CVO tiltmeters and provides another useful signal for checking instrument response.

[119] Wind-associated ground tilt (WAGT) is thought to be caused by atmospheric pressure changes deforming the ground; such pressure changes can be related to the passage of meteorological fronts and, probably more importantly, at least at short periods, air turbulence [*Agnew*, 1986; *Murphy and Savino*, 1975]. Such turbulence must propagate at the wind velocity, and pressure changes vary in strength with the wind [*McDonald and Herrin*, 1975; *Kimball and Lemon*, 1970]. Here we examine wind noise in the 30 s to 10 min period band. For winds moving no faster than tens of km/s, ground deformation should be quasi-static at these frequencies (see $g/\omega c$ relation in section A2).

[120] The amplitude of WAGT varied both temporally and across the tilt network at MSH, but some stations consistently recorded higher amplitudes than others, in some cases exceeding 1 μrad. These stations (NDM, REM, and GLA) tended to record tilts along a clear, dominant tilt azimuth (using terminology introduced in section 4.2, they displayed high linear polarization), and the dominant source azimuth changed little between different windy days. Other stations recorded tilt from a wider range of azimuths except during particularly high-amplitude wind shaking; this may suggest that the linear polarization was a function of signal-to-noise ratio. The constancy of azimuths recorded at some stations over time suggests that atmospheric pressure fluctuations cause the local ground to move in a predictable way, perhaps related to topography or material properties. However, we observe a general lack of temporal correlation between distant stations, probably because pressure disturbances require time for propagation and may affect different sites differently.

[121] Because we expect spatial variations in WAGT we cannot confidently use it to compare instrument response across the network. For example, SEP recorded poor linear polarization, scattered tilt azimuths, and a low amplitude, while just a few hundred meters away station REM recorded very strong polarization, highly consistent azimuths, and high-amplitude response. However, WAGT is a useful signal for comparing colocated instruments. GCL and GCP agreed fairly well with one another, while behavior at North Dome was quite different. Here, NDL recorded amplitudes only 1/5 to 1/10 as large as those at NDM (similar to the ratio observed for episodic tilt) and the dominant tilt azimuths differed by nearly 90°. However, after normalizing and rotating to bring the time series into alignment, the stations agreed very closely along the direction of most intense wind shaking (Figure A7).

[122] In global coordinates, wind-associated ground tilt for 7 different days in which the tilt trajectories displayed strong linear polarization averaged 342° ± 8°, while episodic events during summer 2006 averaged 351° ± 5.5°. This observation, in part, inspired concern that NDM was somehow "locked" into a fixed source azimuth, and motivated the physical rotation of the instrument described in section A6.

A6. Tiltmeter Rotations

[123] To discriminate between instrument and local site effects, tiltmeters NDM and NDL were rotated in their borehole in late May 2008 (NDM ~ 41° clockwise and NDL ~ 33° counterclockwise). We examined the apparent rotation of diurnal ground tilt and wind-induced ground tilt on both instruments (episodic tilts were no longer present at this time), and found that within uncertainties the rotation of apparent tilt azimuths on both tiltmeters were consistent with physical instrument rotations. This result strongly suggests that sensor malfunction was not to blame for (in particular) the different WAGT azimuths recorded at NDM and NDL (section A5), and that instead local site conditions biased one or both data sets.

A7. Conclusions

[124] All instruments appear to have operated correctly, albeit subject to well-known tiltmeter uncertainties such as unpredictable long-term behavior, with an important exception: the two North Dome stations agreed for certain kinds of tilt signals, and disagreed quite strongly for others. NDL and NDM agreed either well or reasonably well for teleseismic and microseismic waves (excepting a rotational misalignment of NDL = NDM + ~10°), diurnal tilts (misalignment of +~30°), episodic tilt azimuths (when actually detected at NDL, the misalignment averaged +~20°), and WAGT (but only after rotating and normalizing the amplitudes). The two stations disagreed for episodic tilt amplitudes, WAGT tilt azimuths and amplitudes (misalignment of ~90°), and very long period ground tilt. Finally, station NDM seemed to record both wind and episodic tilts from a very similar azimuth.

[125] To what can we attribute these issues? Both instruments appear to have operated correctly, as confirmed by teleseismic and microseismic waves and by rotation of the instruments in their borehole. This suggests that the similarity of wind and episodic tilt azimuths at NDM was either coincidental or due to a local site effect. Both Pinnacle and LILY instruments colocated at Guacamole behaved similarly for all detected signals (excluding long-period drift), although they were not in the same borehole and did not record episodic events. And while we note that Pinnacle Series 5000 instruments tended to behave erratically during seismic shaking, this behavior should not have affected episodic tilts of minutes or longer in duration.

[126] The fact that NDL recorded episodic tilt events so poorly is worrying, but the presence of tilts which were spatially and temporally correlated across three stations on the 1980s dome, along with the fact that the episodic tilt events ceased at the end of the eruption, provide very strong evidence that the episodic tilts were real and that NDL failed to properly record them.

[127] It is known that local inhomogeneities can cause strain field distortions which affect local tilt [*Kohl and Levine*, 1993], and it seems likely that the behavior at North Dome was due to such an effect. NDL was installed just beneath the surface, where it would be more sensitive to surface effects and in close proximity to any shallow cracks. We also note again that the relatively thick cable connecting NDM to the surface passed alongside NDL, and the combination was a tight fit in the borehole. It is possible that the cable may have introduced an anisotropy to the tiltmeter response.

[128] Agreement at North Dome for teleseismic and microseismic waves is easily explained by the fact that such signals are generated by tiltmeter accelerations rather than actual deformation that would be affected by an inhomogeneity. It is more difficult to explain the general agreement for diurnal signals. It may be possible that the diurnal deformation signal, if caused by thermal stresses (or possibly in part by tidal stresses), would act over a broad area of the 1980s dome and interact quite differently with a small nearby crack than would the strain field generated by a more localized deformation source such as that which generated the episodic tilts.

[129] More specifically, we hypothesize that an inhomogeneity might have existed to the south of the North Dome borehole, close to the surface, where it would have primarily influenced NDL. In such a location, a small crack would have reduced NDL's north-south sensitivity and might explain the station's poor response to episodic tilt (the source of which lay generally to the south), as well as (very speculatively) its reduced north-south long-period drift. Such a feature might also have altered the apparent source direction for any event which did not occur in line with it and the borehole, and could explain the different tilt azimuths recorded for wind at NDM and NDL.

[130] We conclude that uncertainties associated with episodic volcanic tilt recorded at North Dome may be higher than indicated by the statistics of the data, although this uncertainty is impossible to accurately quantify. But we believe that the data from NDM are more trustworthy than the data from NDL due to the very close agreement of the data with other stations earlier in the eruption, its deeper burial depth, and the much larger amplitude of the recorded tilt signal (it is relatively easy to imagine a mechanism which might decrease the signal-to-noise ratio of an instrument, but more difficult to imagine a mechanism that would artificially increase it).

[131] **Acknowledgments.** We are indebted to numerous colleagues at the Cascades Volcano Observatory for providing data as well as useful comments and assistance with this project. Seth Moran, Evelyn Roeloffs, Alessandro Bonaccorso, Ralf Krug, and Duncan Agnew provided reviews that substantially improved the quality of this work. We also acknowledge invaluable contributions from Riccardo Genco, Dave Sherrod, and Rick LaHusen.

References

Agnew, D. C. (1986), Strainmeters and tiltmeters, *Rev. Geophys.*, *24*(3), 579–624, doi:10.1029/RG024i003p00579.

Aki, K., and P. G. Richards (2002), *Quantitative Seismology*, 700 pp., Univ. Sci. Books, Sausalito, Calif.

Applied Geomechanics Inc. (2007), User's manual: LILY self-leveling borehole tiltmeter, Houston, Tex.

Beauducel, F., F. H. Cornet, E. Suhanto, T. Duquesnoy, and M. Kasser (2000), Constraints on magma flux from displacements data at Merapi Volcano, Java, Indonesia, *J. Geophys. Res.*, *105*, 8193–8203, doi:10.1029/1999JB900368.

Bluth, G. J. S., and W. I. Rose (2004), Observations of eruptive activity at Santiaguito Volcano, Guatemala, *J. Volcanol. Geotherm. Res.*, *136*, 297–302, doi:10.1016/j.jvolgeores.2004.06.001.

Bonaccorso, A., and P. M. Davis (1999), Models of ground deformation from vertical volcanic conduits with application to eruptions of Mount St. Helens and Mount Etna, *J. Geophys. Res.*, *104*, 10,531–10,542, doi:10.1029/1999JB900054.

Bonaccorso, A., G. Falzone, and S. Gambino (1999), An investigation into shallow borehole tiltmeters, *Geophys. Res. Lett.*, *26*, 1637–1640, doi:10.1029/1999GL900310.

Carey, S., and H. Sigurdsson (1985), The May 18 eruption of Mount St. Helens: 2. Modeling of dynamics of the Plinean phase, *J. Geophys. Res.*, *90*, 2948–2958, doi:10.1029/JB090iB04p02948.

Cascades Volcano Observatory (2008), Change in Mount St. Helens alert level and aviation color code, Vancouver, Wash. (Available at http://vulcan.wr.usgs.gov/Volcanoes/MSH/Eruption04/Monitoring/February2008/)

Cashman, K. V., C. R. Thornber, and J. S. Pallister (2008), From dome to dust: shallow crystallization and fragmentation of conduit magma during the 2004–2006 dome extrusion of Mount St. Helens, Washington, in *A Volcano Rekindled: The Renewed Eruption of Mount St. Helens, 2004–2006*, edited by D. R. Sherrod, W. E. Scott, and P. H. Stauffer, *U.S. Geol. Surv. Prof. Pap.*, 1750, 387–413.

Chadwick, W. W., Jr., R. J. Archuleta, and D. A. Swanson (1988), The mechanics of ground deformation precursory to dome-building extrusions at Mount St. Helens 1981–1982, *J. Geophys. Res.*, *93*(B5), 4351–4366, doi:10.1029/JB093iB05p04351.

Denlinger, R. P., and R. P. Hoblitt (1999), Cyclic eruptive behavior of silicic volcanoes, *Geology*, *27*(5), 459–462, doi:10.1130/0091-7613(1999)027<0459:CEBOSV>2.3.CO;2.

Dzurisin, D., J. A. Westphal, and D. J. Johnson (1983), Eruption prediction aided by electronic tiltmeter data at Mount St. Helens, *Science*, *221*(4618), 1381–1383, doi:10.1126/science.221.4618.1381.

Dzurisin, D., M. Lisowski, M. P. Poland, D. R. Sherrod, and R. G. LaHusen (2008), Constraints and conundrums resulting from ground-deformation measurements made during the 2004–2005 dome-building eruption of Mount St. Helens, Washington, in *A Volcano Rekindled: The Renewed Eruption of Mount St. Helens, 2004–2006*, edited by D. R. Sherrod, W. E. Scott, and P. H. Stauffer, *U.S. Geol. Surv. Prof. Pap.*, 1750, 281–300.

Gerlach, T. M., K. A. McGee, and M. P. Doukas (2008), Emission rates of CO_2, SO_2, and H_2S, scrubbing, and preeruption excess volatiles at Mount St. Helens, 2004–2005, in *A Volcano Rekindled: The Renewed Eruption of Mount St. Helens, 2004–2006*, edited by D. R. Sherrod, W. E. Scott, and P. H. Stauffer, *U.S. Geol. Surv. Prof. Pap.*, 1750, 543–571.

Green, D. N., J. Neuberg, and V. Cayol (2006), Shear stress along the conduit wall as a plausible source of tilt at Soufrière Hills volcano, Montserrat, *Geophys. Res. Lett.*, *33*, L10306, doi:10.1029/2006GL025890.

Harrington, R. M., and E. E. Brodsky (2007), Volcanic hybrid earthquakes that are brittle-failure events, *Geophys. Res. Lett.*, *34*, L06308, doi:10.1029/2006GL028714.

Hastings, W. K. (1970), Monte Carlo sampling methods using Markov chains and their applications, *Biometrika*, *57*(1), 97–109, doi:10.1093/biomet/57.1.97.

Iverson, R. M., et al. (2006), Dynamics of seismogenic volcanic extrusion at Mount St. Helens in 2004–05, *Nature*, *444*(7118), 439–443, doi:10.1038/nature05322.

Kimball, B. A., and E. R. Lemon (1970), Spectra of air pressure fluctuations at the soil surface, *J. Geophys. Res.*, *75*(33), 6771–6777, doi:10.1029/JC075i033p06771.

Kohl, M. L., and J. Levine (1993), Measuring low frequency tilts, *J. Res. Natl. Inst. Stand. Technol.*, *98*(2), 191–202.

LaHusen, R. G., K. J. Swinford, M. Logan, and M. Lisowski (2008), Instrumentation in remote and dangerous settings; Examples using data from GPS "Spider" deployments during the 2004–2005 eruption of Mount St. Helens, Washington, in *A Volcano Rekindled: The Renewed Eruption of Mount St. Helens, 2004–2006*, edited by D. R. Sherrod, W. E. Scott, and P. H. Stauffer, *U.S. Geol. Surv. Prof. Pap.*, 1750, 335–345.

Langbein, J., and H. Johnson (1997), Correlated errors in geodetic time series: Implications for time-dependent deformation, *J. Geophys. Res.*, *102*(B1), 591–603, doi:10.1029/96JB02945.

Lensky, N. G., R. S. J. Sparks, O. Navon, and V. Lyakhovsky (2008), Cyclic activity at Soufriere Hills Volcano, Montserrat: Degassing-induced pressurization and stick-slip extrusion, in Fluid Motions in *Volcanic Conduits: A Source of Seismic and Acoustic Signals*, edited by S. J. Lane and J. S. Gilbert, *Geol. Soc. Spec. Publ.*, 307, 169–188, doi:10.1144/SP307.10.

Levine, J., C. Meertens, and R. Busby (1989), Tilt observations using borehole tiltmeters: 1. Analysis of tidal and secular tilt, *J. Geophys. Res.*, *94*(B1), 574–586, doi:10.1029/JB094iB01p00574.

Lisowski, M., D. Dzurisin, R. P. Denlinger, and E. Y. Iwatsubo (2008), Analysis of GPS-measured deformation associated with the 2004–2006 dome-building eruption of Mount St. Helens, Washington, in *A Volcano Rekindled: The Renewed Eruption of Mount St. Helens, 2004–2006*, edited by D. R. Sherrod, W. E. Scott, and P. H. Stauffer, *U.S. Geol. Surv. Prof. Pap.*, 1750, 301–333.

Mastin, L. G., E. Roeloffs, N. M. Beeler, and J. E. Quick (2008), Constraints on the size, overpressure, and volatile content of the Mount St. Helens magma system from geodetic and dome-growth measurements during the 2004–2006+ eruption, in *A Volcano Rekindled: The Renewed Eruption of Mount St. Helens, 2004–2006*, edited by D. R. Sherrod, W. E. Scott, and P. H. Stauffer, *U.S. Geol. Surv. Prof. Pap.*, 1750, 461–478.

McDonald, J. A., and E. Herrin (1975), Properties of pressure fluctuations in an atmospheric boundary layer, *Boundary Layer Meteorol.*, *8*, 419–436, doi:10.1007/BF02153561.

Meertens, C. M., and J. M. Wahr (1986), Topographic effect on tilt, strain and displacement measurements, *J. Geophys. Res.*, *91*(B14), 14,057–14,062, doi:10.1029/JB091iB14p14057.

Metropolis, N., A. W. Rosenbluth, M. N. Rosenbluth, A. H. Teller, and E. Teller (1953), Equation of state calculations by fast computing machines, *J. Chem. Phys.*, *21*(6), 1087–1092, doi:10.1063/1.1699114.

Mindlin, R. D. (1936), Force at a point in the interior of a semi-infinite solid, *Physics*, *7*, 195–202, doi:10.1063/1.1745385.

Mogi, K. (1958), Relations between the eruptions of various volcanoes and the deformations of the ground surfaces around them, *Bull. Earthquake Res. Inst. Univ. Tokyo*, *36*, 99–134.

Moran, S. C., S. D. Malone, A. I. Qamar, W. A. Thelen, A. K. Wright, and J. Caplan-Auerbach (2008a), Seismicity associated with renewed dome building at Mount St. Helens, 2004–2005, in *A Volcano Rekindled: The Renewed Eruption of Mount St. Helens, 2004–2006*, edited by D. R. Sherrod, W. E. Scott, and P. H. Stauffer, *U.S. Geol. Surv. Prof. Pap.*, 1750, 27–54.

Moran, S. C., R. S. Matoza, M. A. Garcés, M. A. H. Hedlin, D. Bowers, W. E. Scott, D. R. Sherrod, and J. W. Vallance (2008b), Seismic and acoustic recordings of an unusually large rockfall at Mount St. Helens, Washington, *Geophys. Res. Lett.*, *35*, L19302, doi:10.1029/2008GL035176.

Mori, J., R. A. White, D. H. Harlow, P. Okubo, J. A. Power, R. P. Hoblitt, E. P. Laguerta, A. Lanuza, and B. C. Bautista (1996), Volcanic earthquakes following the 1991 climactic eruption of Mount Pinatubo: Strong seismicity during a waning eruption, in *Fire and Mud: Eruptions and lahars of Mount Pinatubo, Philippines*, pp. 339–350, Philippine Inst. of Volcanol. and Seismol., Quezon City.

Mortensen, C. E., and D. G. Hopkins (1987), Tiltmeter measurements in Long Valley Caldera, California, *J. Geophys. Res.*, *92*(B13), 13,767–13,776, doi:10.1029/JB092iB13p13767.

Murphy, A. J., and J. M. Savino (1975), A comprehensive study of long-period (20 to 200 seconds) earth noise at the high-gain worldwide seismograph stations, *Bull. Seismol. Soc. Am.*, *65*(6), 1827–1862.

Nakada, S., H. Shimizu, and K. Ohta (1999), Overview of the 1990–1995 eruption at Unzen Volcano, *J. Volcanol. Geotherm. Res.*, *89*, 1–22, doi:10.1016/S0377-0273(98)00118-8.

Nishimura, T., M. Ichihara, and S. Ueki (2006), Investigation of the Onikobe geyser, NE Japan, by observing the ground tilt and flow parameters, *Earth Planets Space*, *58*, e21–e24.

Okada, Y. (1985), Surface deformation due to shear and tensile faults in a half-space, *Bull. Seismol. Soc. Am.*, *75*(4), 1135–1154.

Pallister, J. S., C. R. Thornber, K. V. Cashman, M. A. Clynne, H. A. Lowers, C. W. Mandeville, I. K. Brownfield, and G. P. Meeker (2008), Petrology of the 2004–2006 Mount St. Helens lava dome—Implications for magmatic plumbing and eruption triggering, in *A Volcano Rekindled: The Renewed Eruption of Mount St. Helens, 2004–2006*, edited by D. R. Sherrod, W. E. Scott, and P. H. Stauffer, *U.S. Geol. Surv. Prof. Pap.*, 1750, 647–702.

Scandone, R., and S. D. Malone (1985), Magma supply, magma discharge and readjustment of the feeding system of Mount St. Helens during 1980, *J. Volcanol. Geotherm. Res.*, *23*(3–4), 239–262, doi:10.1016/0377-0273(85)90036-8.

Schilling, S. P., R. A. Thompson, J. A. Messerich, and E. Y. Iwatsubo (2008), Use of digital aerophotogrammetry to determine rates of lava dome growth, Mount St. Helens, 2004–2005, in *A Volcano Rekindled: The Renewed Eruption of Mount St. Helens, 2004–2006*, edited by D. R. Sherrod, W. E. Scott, and P. H. Stauffer, *U.S. Geol. Surv. Prof. Pap.*, 1750, 145–167.

Scott, W. E., D. R. Sherrod, and C. A. Gardner (2008), Overview of the 2004 to 2006, and Continuing, Eruption of Mount St. Helens, Washington, in *A Volcano Rekindled: The Renewed Eruption of Mount St. Helens, 2004–2006*, edited by D. R. Sherrod, W. E. Scott, and P. H. Stauffer, *U.S. Geol. Surv. Prof. Pap.*, 1750, 3–22.

Segall, P. (2010), *Earthquake and Volcano Deformation*, 432 pp., Princeton Univ. Press, Princeton, N. J.

Thelen, W. A., R. S. Crosson, and K. C. Creager (2008), Absolute and relative locations for earthquakes at Mount St. Helens, Washington using continuous data: implications for magmatic processes, in *A Volcano Rekindled: The Renewed Eruption of Mount St. Helens, 2004–2006*, edited by D. R. Sherrod, W. E. Scott, and P. H. Stauffer, *U.S. Geol. Surv. Prof. Pap.*, 1750, 71–95.

Vallance, J. W., D. J. Schneider, and S. P. Schilling (2008), Growth of the 2004–2006 lava-dome complex at Mount St. Helens, Washington, in *A Volcano Rekindled: The Renewed Eruption of Mount St. Helens, 2004–2006*, edited by D. R. Sherrod, W. E. Scott, and P. H. Stauffer, *U.S. Geol. Surv. Prof. Pap.*, 1750, 169–207.

Voight, B., R. P. Hoblitt, A. B. Clarke, A. B. Lockhart, A. D. Miller, L. Lynch, and J. McMahon (1998), Remarkable cyclic ground deformation monitored in real-time on Montserrat, and its use in eruption forecasting, *Geophys. Res. Lett.*, *25*(18), 3405–3408, doi:10.1029/98GL01160.

Voight, B., et al. (1999), Magma flow instability and cyclic activity at Soufriere Hills Volcano, Montserrat, British West Indies, *Science*, *283*, 1138–1142, doi:10.1126/science.283.5405.1138.

Waite, G. P., B. A. Chouet, and P. B. Dawson (2008), Eruption dynamics at Mount St. Helens imaged from broadband seismic waveforms: Interaction of the shallow magmatic and hydrothermal systems, *J. Geophys. Res.*, *113*, B02305, doi:10.1029/2007JB005259.

Watson, I. M., et al. (2000), The relationship between degassing and ground deformation at Soufriere Hills Volcano, Montserrat, *J. Volcanol. Geotherm. Res.*, *98*, 117–126, doi:10.1016/S0377-0273(99)00187-0.

Widiwijayanti, C., A. Clarke, D. Elsworth, and B. Voight (2005), Geodetic constraints on the shallow magma system at Soufrière Hills Volcano, Montserrat, *Geophys. Res. Lett.*, *32*, L11309, doi:10.1029/2005GL022846.

Wyatt, F., G. Cabaniss, and D. C. Agnew (1982), A comparison of tiltmeters at tidal frequencies, *Geophys. Res. Lett.*, *9*(7), 743–746, doi:10.1029/GL009i007p00743.

Wyatt, F. K., S. Morrissey, and D. C. Agnew (1988), Shallow borehole tilt: A reprise, *J. Geophys. Res.*, *93*(B8), 9197–9201, doi:10.1029/JB093iB08p09197.

Wylie, J. J., B. Voight, and J. A. Whitehead (1999), Instability of magma flow from volatile-dependent viscosity, *Science*, *285*(5435), 1883–1885, doi:10.1126/science.285.5435.1883.

Yang, X. M., P. M. Davis, and J. H. Dieterich (1988), Deformation from inflation of a dipping finite prolate spheroid in an elastic half-space as a model for volcanic stressing, *J. Geophys. Res.*, *93*(B5), 4249–4257, doi:10.1029/JB093iB05p04249.

K. Anderson and P. Segall, Department of Geophysics, Stanford University, 397 Panama Mall, Stanford, CA 94305, USA. (kander@stanford.edu)

M. Lisowski, USGS Cascades Volcano Observatory, 5400 MacArthur Blvd., Vancouver, WA 98683, USA.